Chapter 3

Thermal relaxation of polyvinyl acetate near glass transition temperature - a micro-Raman study

3.1 Introduction

Polymer thin films and polymer coatings are extensively used as antibacterial/antiviral surfaces, superhydrophobic surfaces, and also in devices such as switches, sensors and capacitors, and solar cells composed of perovskite, conducting polymer, and dye, in the form of corrosion-resistant coatings[1, 2, 3, 4]. The working temperature of these polymer film-based devices can be in the vicinity of their glass transition temperature, so the existence of some of these polymers in the glassy state is unavoidable. During these applications, the polymer is subjected to electrical, mechanical, or thermal perturbations [5, 6, 7, 8, 9, 10]. A study of the glassy state and in particular, the response of these polymer films to thermal perturbations is necessary to fabricate long-lasting devices with stable, reproducible performance. The response of polymer films to thermal perturbation crossing the glass transition temperature of the polymer is a complex phenomenon and has widely been studied through experimental, computational, and theoretical approaches [11, 12, 13].

The glassy state is popularly defined as a state in which the polymer has a morphology similar to any crystalline solid but the molecular arrangement in the polymer is disordered like liquids. In the glassy state, a polymer is away from equilibrium and slowly relaxes toward the equilibrium crystalline state.

This relaxation of polymer towards its equilibrium state becomes slower with the passage of time. This phenomenon is known as aging and the polymer relaxation times are often found to be exceeding the experimental timescales [11, 13]. During relaxation towards an equilibrium crystalline state, the polymer often contains domains with variable ordered structures which in turn results in spatiotemporal heterogeneities [14]. The Adam Gibbs theory was the first to analyze the relaxation dynamics of glasses in terms of these domains which were termed cooperatively rearranging regions (CRRs). Adam and Gibbs predicted that the size of these CRRs has a temperature dependence and this theory has been widely supported by several experimental results, but the Adam and Gibbs theory lacks the explanation of heterogeneities in these CRRs [15]. The random first order theory (RFOT) showed that the dynamic heterogeneities are due to a mosaic of CRRs which are due to several local metastable states in the free energy landscape of a glass former. This theory was successful in explaining the relaxation dynamics of the glassy system for a wide variety of glass formers experimentally [16].

The relaxation of polymers in response to external perturbations is often studied as a variation in thermal and mechanical stress in a glassy regime which is due to the aging response of the polymer. Thus, aging in polymer glasses is an important parameter that not only governs the polymer dynamics but also the polymer processing of bulk polymer and polymer film-coated device performance. It has been reported that the thermal response dynamics of the unprocessed or bulk glassy state is different than that of the processed or film state of the polymer glass [17, 18, 19, 20]. Most of these differences arise due to the presence of free surface and confinement effects in films, with relaxations near the film surface often completely different compared to those in the bulk state [20].

There are conflicting views on differences in glass transition temperature in polymers on the free surface of films, near surfaces, interfaces and in nanoconfinement, [21], with most experiments reporting a clear decrease in glass transition temperature as a function of film thickness [22, 23], whereas some studies have reported no change in T_g [24, 25], or an increase in T_g under extreme confinement [26]. Nanoindentation, diffusion, and fluorescence experiments have demonstrated that below the glass transition temperature, the polymer film surface is more fluid-like with enhanced mobility and relaxation

dynamics compared to the bulk [20, 27, 28, 29]. Moreover, the activation energy of the relaxation processes near the film surface is significantly less than the bulk value [27]. Above T_g, the film dynamics largely resemble the bulk molecular relaxation dynamics. A key observation is a decoupling of surface diffusion dynamics from the relaxation processes near the surface in films [27].

Since macroscale response is governed by the processes that happen at the molecular level, it is crucial to analyze these molecular-scale differences between bulk and film surface by monitoring molecular dynamics [30]. This is especially important when the film is used for coating because surface effects in glassy polymer films can change adhesion and friction at the surface, or in advanced polymer-based lithography, surface tension and wetting or transferability can change at very small length scales, leading to problems. Because of the large inherent length scales in polymers and slow dynamics near the glass transition, leading to a large spread of time scales, molecular dynamics simulations of these polymer glasses are very challenging. Nevertheless, some coarse-grained and atomistic simulation models have addressed the questions concerning polymers near the glass transition, especially in confinement [18, 31, 32]. A convenient way to study glassy state dynamics is through the changes in the vibrational modes of the different chemical bonds constituting the polymer molecule with the help of micro-Raman spectroscopy, which decouples the different molecular modes, permitting the observation of the dynamics of a particular mode of interest. We have attempted to understand the thermodynamics and kinetics near the glassy state using Raman mode relaxations of the main chain (skeletal) and in the side branches of PVAc. Our studies reveal significant differences in the molecular-scale relaxation processes in the film and the unprocessed PVAc as they are subjected to thermal cycles passing through the T_g. The differences in the glassy state kinetics are also found to depend on the mode of approach to T_g. We provide experimental evidence of the presence of cooperative rearranging regions, and our observations are better explained by the RFOT rather than the Adam Gibbs theory.

3.2 Preparation of polymer film

Poly(vinyl) acetate (PVAc) of molecular weight 50,000 M was purchased from Alfa Aesar and was used without further treatment as the unprocessed state of

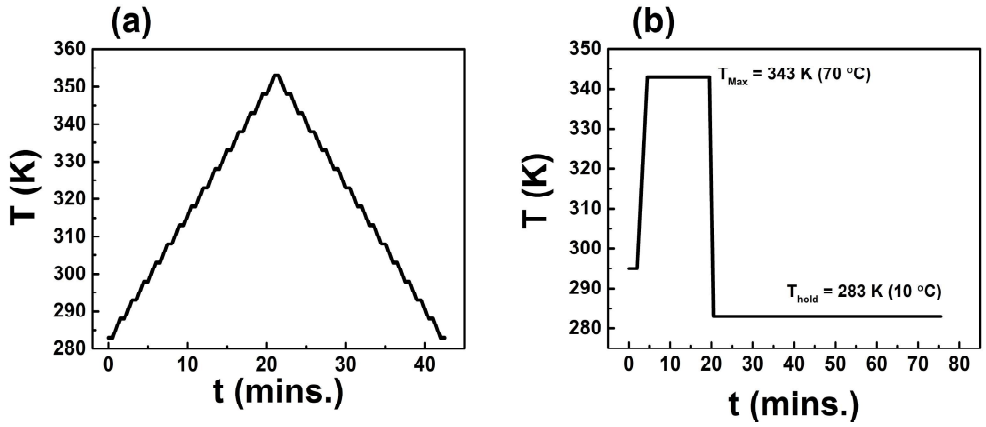

FIGURE 3.1: (a) The thermal ramp applied to the polymer in both unprocessed and film state (b) The thermal quench applied to the polymer, T_{Max} is the maximum temperature to which the films were heated and T_{hold} is the temperature at which the films were maintained after quenching.

PVAc. For the preparation of PVAc film, 20% by weight of PVAc was dissolved in 99.9% pure acetone (purchased from LOBA chemicals) in a ratio such that the resultant solution is 10 ml in volume. The solution was blended by constant stirring at room temperature on a magnetic stirrer for 60 minutes. After 60 minutes, the solution was drop casted on a glass substrate (thoroughly cleaned with chromic acid and dried at room temperature). The PVAc film was left to dry for 24 hours at room temperature before the experiment. The thickness of the film was measured to be 0.38 mm (approx. 380 μm).

3.3 Raman spectroscopy

The instrumental and theoretical details of Raman spectroscopy have already been discussed in Chapter 2, section 2.5. To study the thermal relaxation of a glassy polymer, PVAc in both unprocessed and film state was subjected to two different thermal cycles: thermal ramp and thermal quench passing through the glass transition temperature.

3.4 Methodology for thermal perturbation

3.4.1 Thermal ramp

Two temperature ramp cycles from 293 K to 343 K (20 °C to 70 °C) for unprocessed PVAc and from 283 K to 353 K (10 °C to 80 °C) for PVAc film were applied. For unprocessed PVAc, the Raman spectrum was recorded at steps of 10 K each during both heating and cooling cycles and for PVAc film, the Raman spectrum was recorded at steps of 10 K for the first ramp and at the steps of 5 K for the second ramp cycle. The rate of heating and cooling was set to 10 K/min for both bulk PVAc and PVAc film. The sample was not maintained at any temperature for a duration longer than the time required for its acquisition. A typical thermal ramp for PVAc film is shown in Figure 3.1(a) for the second ramp cycle applied. The range of the temperature ramp cycle was chosen such that each cycle crosses the T_g of the polymer. The first ramp cycle was mainly performed to anneal the sample so that any thermal history can be erased and to evaporate moisture content or solvent present in the sample.

3.4.2 Thermal quench

The thermal quench applied to both unprocessed PVAc and PVAc film is shown in Figure 3.1(b). A Raman spectrum was collected at room temperature at the beginning of the thermal cycle. Then the sample was heated up to T_{Max} at the rate of 20 K/min and was maintained at the same temperature for 15 minutes. Heating the samples up to T_{Max} was done to erase any thermal history present within the polymer film. Raman spectrum was also collected at T_{Max}. After 15 minutes the sample was quenched with two different quenching rates of 60 °C/min and 100 °C/min up to T_{hold} = 10 °C. After quenching the sample was maintained at the same temperature (T_{hold}) for 60 minutes. Raman spectrum was collected as a function of waiting time after quench (t_w) at an interval of 5 minutes from 0 minutes to 60 minutes.

3.4.3 Data collection and analysis

The instrument was first calibrated using naphthalene crystal. The data was collected with STP Data Collection Software and was analyzed using Microcal

Origin. The acquired spectrum was auto-subtracted from the background spectrum. The first phase of data analysis included baseline correction of individual Raman spectra for all the experiments by detrending and fitting with a polynomial function which was then subtracted from the original spectrum. The corrected data were then used for further analysis. All the peaks appearing in the Raman spectrum were individually analyzed using non-linear least square fitting with Gaussian (3.1), Lorentzian (3.2), and Voigt (3.3) functions. The best fit was determined for all the peaks and the following parameters were obtained: peak center, peak height, peak area, and peak full width at half maximum (FWHM).

$$I = I_0 + A\frac{\exp\frac{-4\ln(2)(x-x_c)^2}{w^2}}{w\sqrt{\frac{\pi}{4\ln(2)}}} \tag{3.1}$$

$$I = I_0 + \frac{2Aw}{4\pi(x-x_c)^2 - w^2} \tag{3.2}$$

$$I = I_0 + A\frac{2ln(2)w_L}{\pi^3/2w_G^2}\int_{-\infty}^{\infty}\frac{x^2}{(\frac{w_L}{w_G}\sqrt{\ln(2)})^2 + (\frac{x-x_c}{w_G}\sqrt{4\ln(2)})^2 dt} \tag{3.3}$$

In the above equations, I is the Raman intensity, I_o is constant, x represents the Raman shift (in cm^{-1}), x_c is the Raman peak center (in cm^{-1}), w is the full width at half maximum (FWHM in cm^{-1}), and A is the area under the peak. For equation 3.3, w_G is the Gaussian FWHM and w_L is the Lorentzian FWHM.

3.5 Raman spectrum of unprocessed PVAc and PVAc film

The Raman spectrum at room temperature for unprocessed PVAc is shown in Figure 3.2(a). In the unprocessed state, the Raman spectrum of PVAc contains sharp peaks with the highest peak at around 2800 cm^{-1} - 3100 cm^{-1} representing the C-H stretching vibrational modes. The peaks in the Raman spectrum of unprocessed PVAc are labeled in Figure 3.2 (a) and the inset shows the closely appearing bands which can be deconvoluted into the respective Raman peaks. Figure 3.2(b) shows two closely appearing Raman peaks which are deconvoluted into peak 1 and peak 2 using the Lorentzian function

(Equation 3.2) with peak centers at 1023 cm^{-1}, corresponding to C-H bending / CH_2 twisting and at 1126 cm^{-1} corresponding to C-C stretching modes. Peaks 3, 4, 5, and 6 are deconvoluted from a band between 1200 cm^{-1} to 1450 cm^{-1}. Peak 3 centered at 1277 cm^{-1} corresponds to C-H bending / C-H deformation modes. Peak 4 and peak 5 centered at 1350 cm^{-1} and 1375 cm^{-1} correspond respectively to CH_2 symmetric deformation and CH_3 asymmetric deformation. The most intense peak in the band is peak 6 at 1438 cm^{-1} corresponding to CH_2 deformation/ scissoring. Peak 7 centered at 1735 cm^{-1} corresponds to C=O symmetric stretching and is very prominently observed in the Raman spectra of unprocessed PVAc. Since it is a part of the acetate group in the side chain, it can give important information on side chain relaxation. Lastly, the C-H stretching region around 2800 cm^{-1} - 3100 cm^{-1} representing the C-H stretching vibrational modes is deconvoluted into 4 peaks with the most intense peak occurring at 2940 cm^{-1} corresponding to C-H asymmetric Stretching in CH_2 group of the main chain, and so it can throw light on the main chain dynamics. The peaks at 2984 and 2857 cm^{-1} corresponding respectively to C-H asymmetric stretching and C-H symmetric stretching in CH_3 group of the side chain are relatively very weak. A very weak broad peak is also observed at 3025 cm^{-1} which can be due to other C-H stretching modes present in the main chain and side chain of the polymer. The vibrational modes corresponding to the peaks in the Raman spectrum of unprocessed PVAc are assigned their respective vibrational modes in Table 3.1 along with the fitting function.

The Raman spectrum of PVAc film at room temperature is shown in Figure 3.3 (a). It is observed that instead of sharp peaks as observed in unprocessed PVAc, the Raman spectrum of PVAc film consisted a broad band in the region 1000 cm^{-1} to 2500 cm^{-1} which contains the contribution of several vibrational modes from the main chain as well as side chain of the polymer. This broad band was deconvoluted into two Raman bands centered at 1377 cm^{-1} and 1572 cm^{-1} as shown in Figure 3.3 (b). A very weak C-C stretching peak is observed sometimes around 1100 cm^{-1}, but many times it merges within the band. Thus, the band contains all the modes corresponding to the main chain and side branch deformations present in the Raman spectrum of unprocessed PVAc. In the C-H stretching region from 2800 cm^{-1} to 3100 cm^{-1}, a single Raman band is observed in PVAc film instead of four sharp peaks occurring in unprocessed PVAc. The C-H stretching peak in PVAc film is centered at 2910 cm^{-1} as shown in Figure 3.3

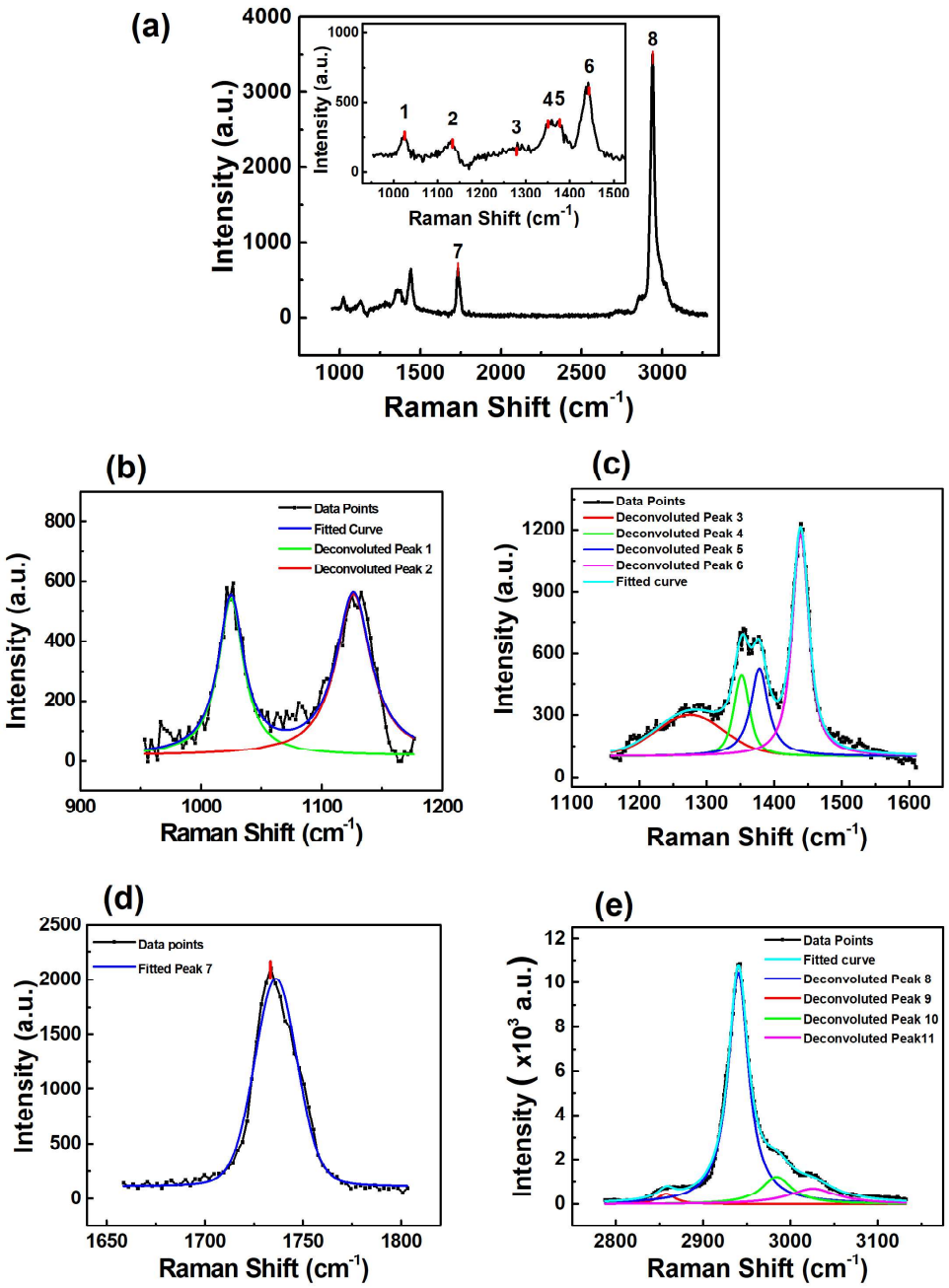

FIGURE 3.2: (a) Raman spectrum at room temperature (25 °C) of unprocessed PVAc representing the vibrational modes presented as peaks in the Raman spectrum. The inset in (a) represents closely appearing Raman bands which can be deconvoluted into various Raman peaks. (b) represents deconvolution of peaks 1 and 2 1023 cm^{-1} and 1126 cm^{-1} using Lorentzian function (Equation 3.2) (c) represents deconvolution of the band between 1150 cm^{-1} to 1600 cm^{-1} into peaks 3, 4, 5 and 6 using Voigt function (Equation 3.3) (d) represents peak 7 at 1735 cm^{-1} fitted using Equation 3.3 and (f) represents deconvolution of Raman band between 2800 cm^{-1} to 3100 cm^{-1} into peaks 8, 9, 10 and 11 using Lorentzian function (Equation 3.2). The peaks are assigned their respective vibrational modes in Table 3.1

TABLE 3.1: Peak assignments and their peak center at room temperature (30 °C) for peaks appearing in unprocessed PVAc. The peak numbers as assigned in Figure 3.2(a). The best fit to the peaks is determined from non-linear least square fitting results. The peaks are assigned their respective vibrational modes with the help of existing literature [34, 36, 37].

Peak No.	Peak center (cm^{-1})	Assignment	Annotation	Character (at 30 °C)
P1	1023	C-H Bending/CH_2 Twisting	vw	Lorentz
P2	1126	C-C Stretching	vw	Lorentz
P3	1277	C-H Bending/ C-H deformation	vw	Voigt, more contribution from Gaussian
P4	1350	CH_2 Symmetric deformation	w	Voigt, more contribution from Gaussian
P5	1375	CH_3 Asymmetric deformation	w	Voigt, more contribution from Lorentz
P6	1438	CH_2 Scissoring + deformation	m-w	Voigt, more contribution from Lorentz
P7	1735	C=O Symmetric Stretching	w	Voigt, more contribution from Gaussian
P8	2940	C-H Asymmetric stretching, CH_2	vs	Lorentz
P9	2857	C-H Symmetric stretching, CH_3	vw	Lorentz
P10	2984	C-H Asymmetric stretching, CH_3	w	Lorentz
P11	3025	C-H Symmetric stretching	vw	Lorentz

(c).

Basically, the sharp Raman peaks observed in unprocessed PVAc were concealed into a broad band in the Raman spectra of the PVAc film. The broadening of Raman bands on casting the polymer into a film is a distinct feature that has not been observed so far. To be certain that the broadening is a property of the polymer and not due to any impurities some control experiments were performed wherein, the Raman spectrum of a blank glass (processed and cleaned without depositing film) was collected, no peaks were observed in the Raman spectrum of glass in the observed spectral range indicating that there is no contribution of the glass substrate in the Raman spectrum of PVAc film. Therefore, band broadening is a consequence of casting the polymer into a film.

When a polymer is casted into a film the polymeric chains can adopt a huge number of different conformations. These different conformations introduce disorders in the polymeric system [33]. The broadening of the Raman spectrum is a consequence of induced disorders in the polymer film. As a result of the increased disorder, the vibrational and rotational energy states of neighboring modes couple and the band becomes broader due to roto-vibrational transitions [34]. These disorders also give rise to localization of states [35] which was verified using UV-Vis spectroscopy and it was observed that instead of a sharp absorption edge, the spectrum contains a tail which indicates that the states are localized.

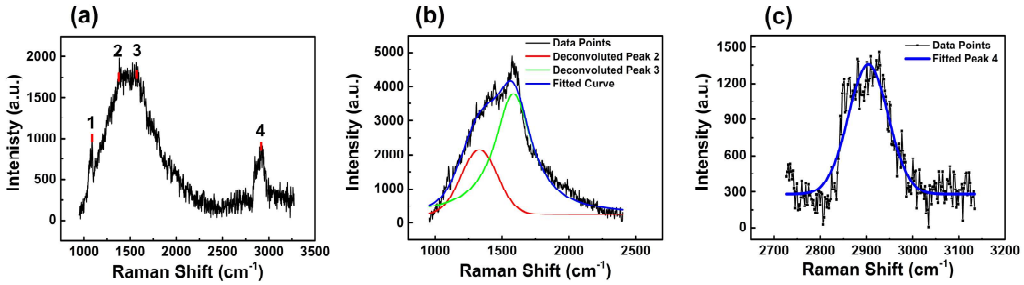

FIGURE 3.3: (a) Raman spectrum of PVAc film at room temperature ($\approx$ 25 °C). (b) broad band appearing in the Raman spectrum of PVAc film, deconvoluted into two peaks using Voigt function (Equation 3.3) and (c) Raman band representing C-H stretching vibrational modes in PVAc film fitted using Lorentzian function (Equation 3.2).

3.6 Effect of thermal ramp

To study the effect of the thermal ramp, the unprocessed and film state of PVAc were subjected to two thermal ramp cycles. A schematic of the temperature ramp cycle is shown in Figure 3.1 (a). A substantial change in the peak fit parameters was observed as a function of temperature during the heating and cooling cycles.

3.6.1 Unprocessed PVAc

The influence of heating and cooling cycles of the thermal ramp on the Raman spectrum of unprocessed PVAc is evident from Figure 3.4. It can be observed that during ramp 1, the peaks are more intense during heating as compared to cooling (Figure 3.4(a)) whereas, during ramp 2, the peaks become more intense during cooling as compared to the heating (Figure 3.4(b)).

To study the overall effect of thermal ramp in unprocessed PVAc, three peaks are selected and the variation in their peak fit parameters is observed as a function of temperature. The selection of peaks was such that it represents the contribution from both the main chain and side branch of the polymer so that the overall behavior of the polymer chain can be observed. The three peaks chosen for further analysis are - Peak 2 corresponding to C-C stretching vibrational modes present in the main chain of the polymer (the backbone of the polymer), Peak 7 corresponding to the C=O stretching mode present in the side chain of the polymer and Peak 8 corresponding to C-H stretching vibrational

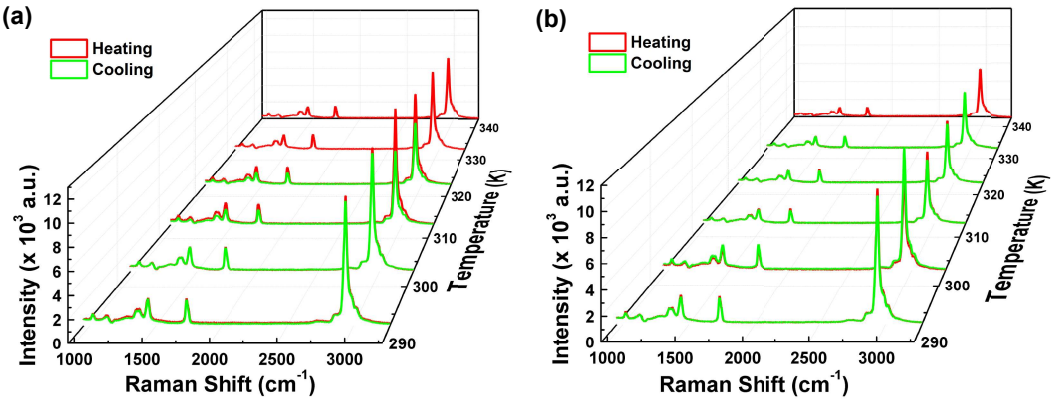

FIGURE 3.4: Effect of temperature ramp (a) ramp 1 and (b) ramp 2 on the Raman spectrum of unprocessed PVAc. A prominent change in the Raman peaks is observed as a function of temperature during the heating (red) and cooling (green) cycles.

modes which are present in both the main chain and the side branch of the polymer.

Figure 3.5 represents the temperature dependence of the peak fit parameters of peak 2 of bulk PVAc, which represents C-C stretching modes present in the main chain of the polymer. A pronounced hysteresis is observed in the maximum peak intensity, I_{Max} (Figure 3.5(b)) and peak area, I_{INT} (Figure 3.5(c)) in the first ramp which decreases during second ramp cycle. There is an overall 5% loss in the recovery of I_{Max} and 11% loss in the recovery of I_{INT} during the thermal ramp. Whereas, the peak FWHM (Figure 3.5(d)) and peak center (Figure 3.5(e)) fluctuates around 40.65 $\pm$ 6.17 cm^{-1} and 1125.44 $\pm$ 1.37 cm^{-1} respectively. The study of C-C stretching vibrations provides information about the relaxation of the main chain (backbone) of the polymer.

To further analyze the thermal response of the side chain of the polymer, peak fit parameters of peak 7 are studied as a function of temperature. The peak represents stretching vibrations of the carbonyl (C=O) functional group, located in the side chain of the polymer. The temperature dependence of peak fit parameters of peak 7 is shown in Figure 3.6. A behavior similar to the main chain C-C stretching vibrations is observed in the I_{Max} Figure 3.6(b) and I_{INT} Figure 3.6(c) of the side chain modes with an overall 3% loss in the recovery for both. A pronounced hysteresis is observed in the ramp 1 (heating-cooling) cycle which is reduced during ramp 2. The FWHM (Figure 3.6(d)) and peak center

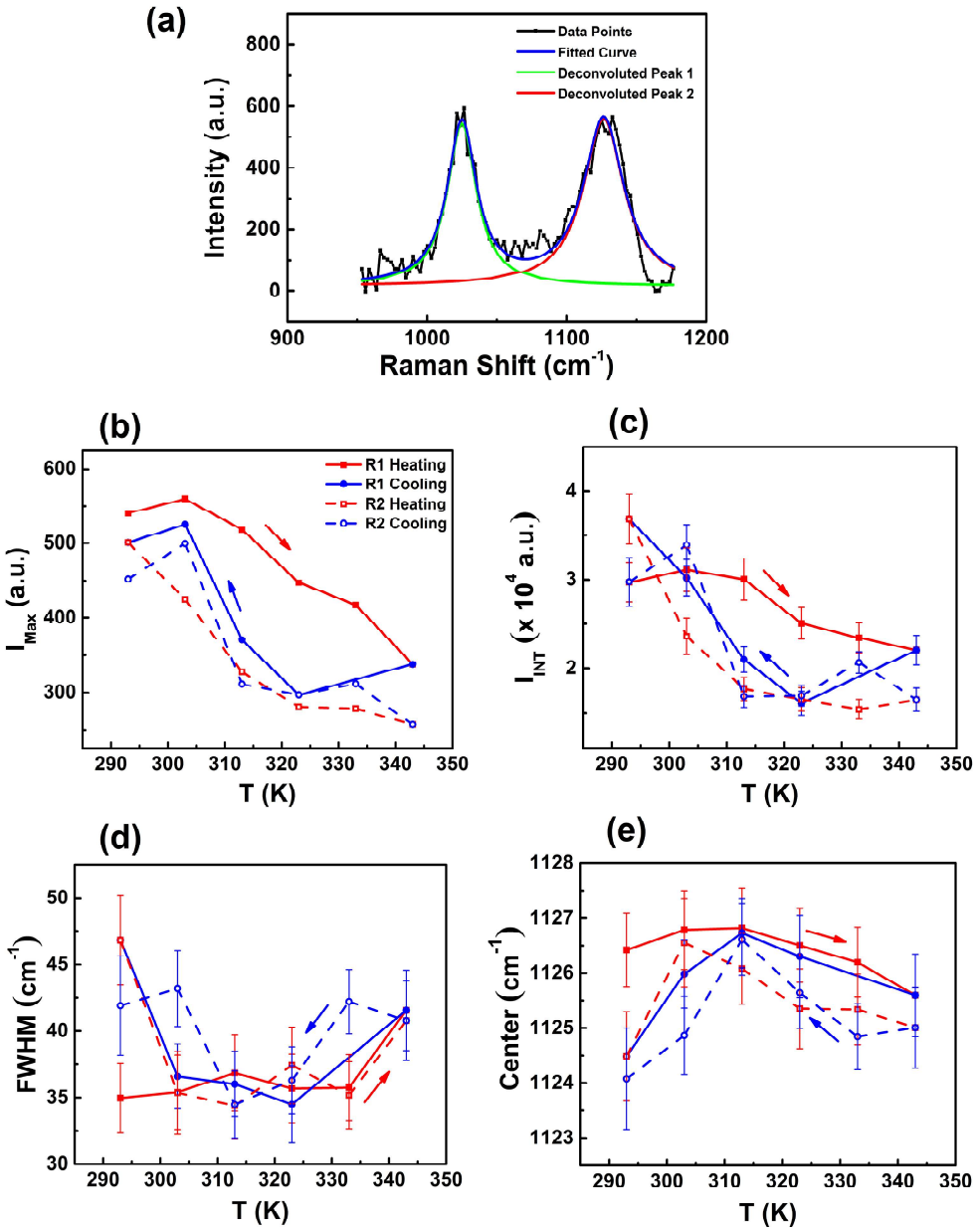

FIGURE 3.5: (a) C-C stretching peak (peak 2) of unprocessed PVAc fitted with Lorentzian function (Equation 3.2) at T = 313 K contributing to the main chain/ backbone of the polymer. Evolution of this peak as a function of temperature for heating (red) and cooling (blue) cycles of ramp 1 (R1, solid) and ramp 2 (R2, dashed) for the peak parameters (b) peak height (I_{Max}), (c) peak area (I_{INT}), (d) FWHM and (e) peak center.

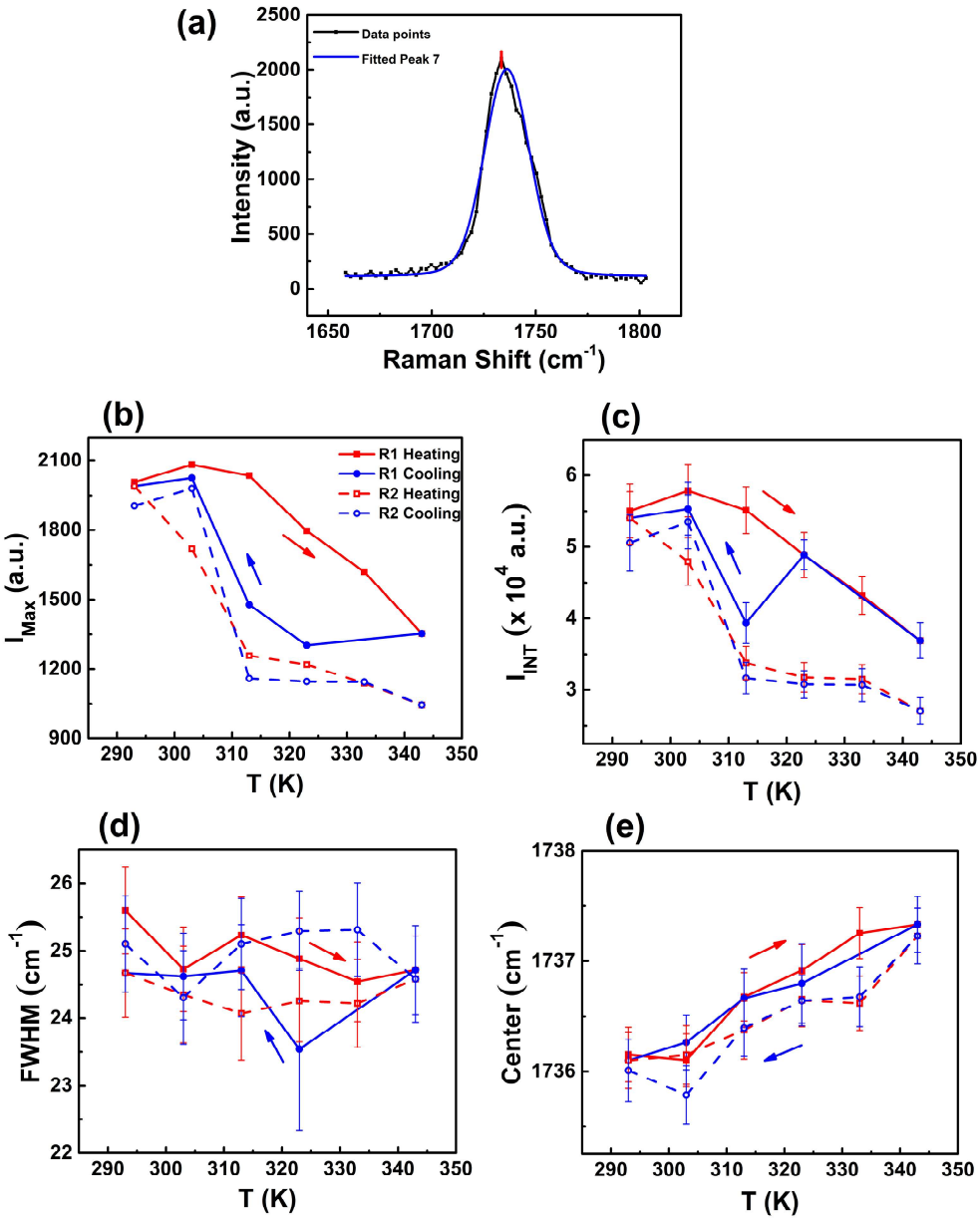

FIGURE 3.6: (a) C=O stretching peak (peak 7) of unprocessed PVAc fitted with Lorentzian function (Equation 3.2) at T = 313 K which contributes to the side branch of the polymer. Influence of temperature ramp during heating (red) and cooling (blue) cycles of ramp 1 (R1, solid) and ramp 2 (R2, dashed) for the peak parameters (b) peak height (I_{Max}), (c) peak area (I_{INT}), (d) FWHM and (e) peak center.

(Figure 3.6(e)) on the other hand remains unaffected by the changing temperature with a slight variation of 24 $\pm$ 1 cm^{-1} and 1736.7 $\pm$ 0.5 cm^{-1} respectively. The vibrational modes present in both the main chain and side chain of the polymer show similar characteristics as a function of temperature indicating that the relaxation in PVAc is cooperative in the unprocessed state.

The most prominent vibrating mode present in the polymer is the C-H stretching mode which appears predominantly between 2800 cm^{-1} to 3100 cm^{-1} of the Raman spectrum of PVAc. The C-H modes are present in the main chain as well as in the side branch of the polymer, and this aspect makes the study of these modes important since they can give signatures of relaxations in both the main and side chains of the polymer. The temperature dependence of peak fit parameters of peak 8 in bulk PVAc which represents the C-H asymmetric stretching vibrations is shown in Figure 3.7. A hysteresis similar to the one present in the C-C vibrations of the main chain and C=O vibrations of the side chain of the polymer is observed in the I_{Max} and I_{INT} of the C-H modes which can be seen in Figure 3.7(b) and 3.7(c) respectively. Around 5% loss is observed in the recovery of I_{Max} and I_{INT}. Alternatively, the peak FWHM (Figure 3.7(d)) and center (Figure 3.7(e)) remain unaltered during the thermal cycle with a slight variation of $\pm$ 0.5 cm^{-1} in both.

3.6.2 PVAc film

The effect of the thermal ramp on the Raman spectrum of PVAc film is more pronounced and evident as compared to unprocessed PVAc which can be seen from Figure 3.8. During the first ramp cycle, as shown in Figure 3.8 (a) it can be seen that the Raman bands are becoming broader and more intense as a function of temperature during heating and cooling cycles. This broadening becomes more pronounced and the Raman bands become more intense during the second ramp cycle which can be seen in Figure 3.8 (b). The Raman bands become 10 times more intense during ramp 2 as compared to ramp 1. Due to the presence of disorders in PVAc film, the thermal ramp crossing the glass transition temperature can drive the system out of its equilibrium which is more prominent as compared to unprocessed PVAc.

From the Raman spectrum, the broad Raman band is deconvoluted into two peaks: peak 2 and peak 3 as shown in Figure 3.9 (a). The effect of the thermal

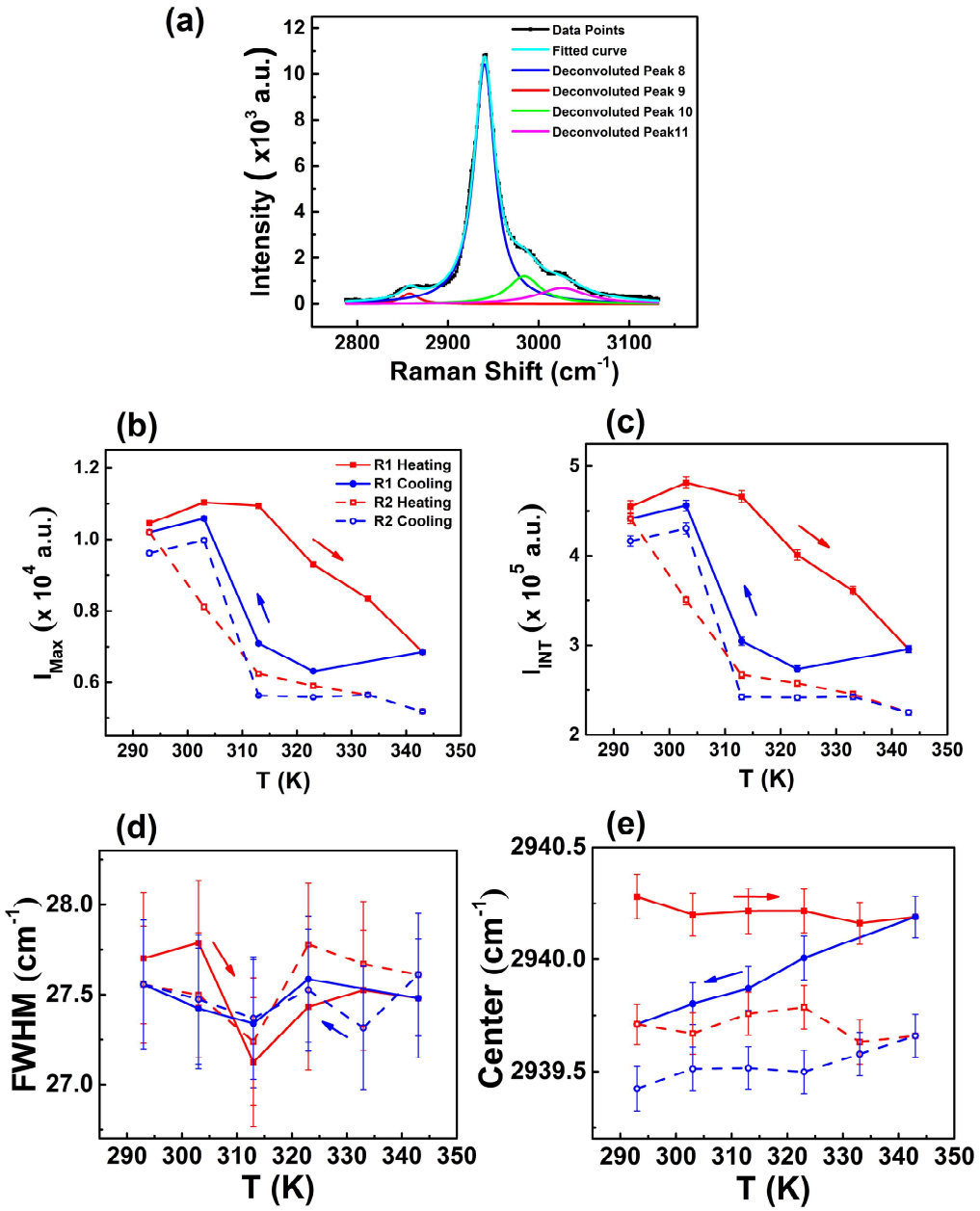

FIGURE 3.7: (a) C-H stretching peak (peak 8) of unprocessed PVAc fitted with Lorentzian function (Equation 3.2) at T = 313 K which contributes to the side branch of the polymer. Influence of temperature ramp during heating (red) and cooling (blue) cycles of ramp 1 (R1, solid) and ramp 2 (R2, dashed) for the peak parameters (b) peak height (I_{Max}), (c) peak area (I_{INT}), (d) FWHM and (e) peak center.

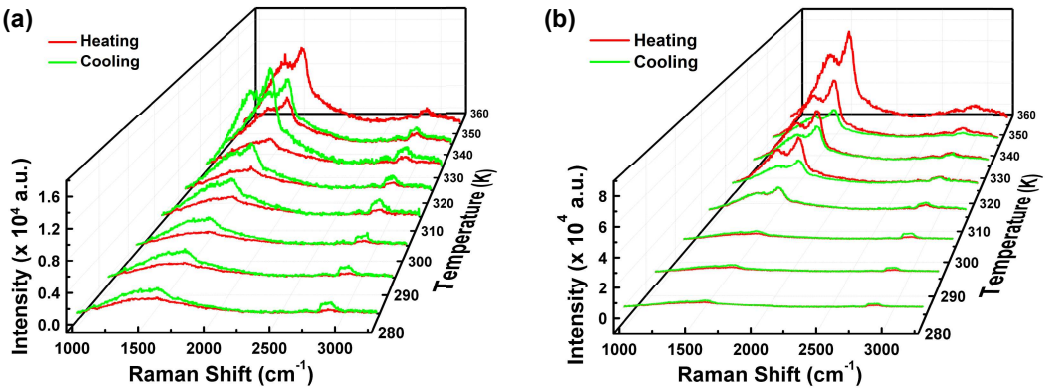

FIGURE 3.8: Effect of temperature ramp (a) ramp 1 and (b) ramp 2 on the Raman spectrum of PVAc film. A prominent change in the Raman peaks is observed as a function of temperature during heating (red) and cooling (green) cycles with a remarkable variation in ramp 2.

ramp is more clear and more evident on analyzing the temperature response of the peak parameters. Similar to unprocessed PVAc, the peaks in PVAc film also follow the hysteresis pattern as a function of heating and cooling temperature cycles. During ramp 1, the I_{Max} shows a hysteresis pattern for both peak 2 and peak 3 with a higher I_{Max} magnitude for peak 3 as shown in Figure 3.9 (b). Similarly, I_{INT} also represents a hysteresis pattern with a higher quantity for peak 3 as compared to peak 2 3.9 (c). Both I_{Max} and I_{INT} increase during the heating cycle and decrease during the cooling cycle. An increase in I_{Max} and I_{INT} indicates, an increase in the concentration of contributing molecules of that vibrational mode in the Raman spectrum. This behavior in PVAc film is just the opposite of the decreasing nature of I_{Max} and I_{INT} of the peaks appearing in unprocessed PVAc. The FWHM of peak 2 and peak 3 in PVAc film shows a decrease with increasing temperature and it increases on decreasing the temperature as shown in Figure 3.9 (d). The hysteretic behavior is also present in FWHM but the hysteresis is more pronounced in peak 3 as compared to peak 2. Peak center on the other hand shows comparatively less variation for both peak 2 and peak 3 (3.10 (e)).

During ramp 2, peak 2 and peak 3 of PVAc film becomes more and more intense with the changing temperature. A representative of peak 2 and peak 3 is shown in Figure 3.10 (a). Both peak 2 and peak 3 show an increase in I_{Max} and I_{INT} with increasing temperature and decrease in I_{Max} and I_{INT} with decreasing

temperature as shown in Figure 3.10 (b) for I_{Max} and in Figure 3.10 (c) for I_{INT}. The hysteresis in ramp 2 is smaller as compared to ramp 1 but the magnitudes of I_{Max} and I_{INT} have increased to 10 times in ramp 2 as compared to ramp 1. The FWHM of peaks shows a decreasing character on heating and an increasing character during cooling as shown in Figure 3.10 (d). Negligible hysteresis is observed in FWHM for both peak 2 and peak 3. The variation in peak center is negligible for peak 2 as well as peak 3 during ramp 2 (Figure 3.10 (e)).

The Raman band containing peaks 2 and peak 3 is a contribution from several vibrational modes (these are present as peak 1 - peak 7 in the Raman spectrum of unprocessed PVAc), which can result in higher intensity and area under the band. However, the C-H stretching vibrational mode has a distinct peak, peak 4 in PVAc film which can provide a more precise interpretation of the effect of the thermal ramp on PVAc film.

The C-H stretching peak and its respective fit in PVAc film are shown in Figure 3.11 (a) and 3.12 (a) for ramp 1 and ramp 2 respectively. During the first ramp, I_{Max} and I_{INT} of peak 4 are observed to increase during the heating cycle and decrease during the cooling cycle as shown in Figure 3.11 (b) and (c) respectively. The C-H stretching mode in PVAc film shows a character similar to the peaks in unprocessed PVAc and opposite to peaks 2 and 3 of PVAc film. There is large hysteresis in I_{Max} and I_{INT} of peak 4 during ramp 1. The FWHM of peak 4 also shows a behavior similar to I_{Max} and I_{INT} with a comparatively smaller hysteresis as shown in Figure 3.11 (d). The peak center of peak 4 also shows a slight shift towards increasing wavenumbers during the heating cycle and a shift towards lower wavenumbers during the cooling cycle (Figure 3.11 (e)).

During ramp 2, the peak parameters of peak 4 show a similar but more pronounced behavior as a function of temperature. The I_{Max} and I_{INT} show a hysteresis with a crossover at 313 K which is the temperature close to T_g of PVAc ($\approx$ 310 K) as shown in Figure 3.12 (b) and (c) respectively for I_{Max} and I_{INT}. This behavior has distinct relationships with the glassy dynamics of the polymer which will be discussed in the last section of this chapter. The FWHM for peak 4 during ramp 2 increases to higher values with increasing temperature and decreases with decreasing temperature, as shown in Figure 3.12 (d) and the peak center shifts towards higher wavenumbers during increasing temperature and towards lower wavenumbers during decreasing temperature Figure 3.12(e).

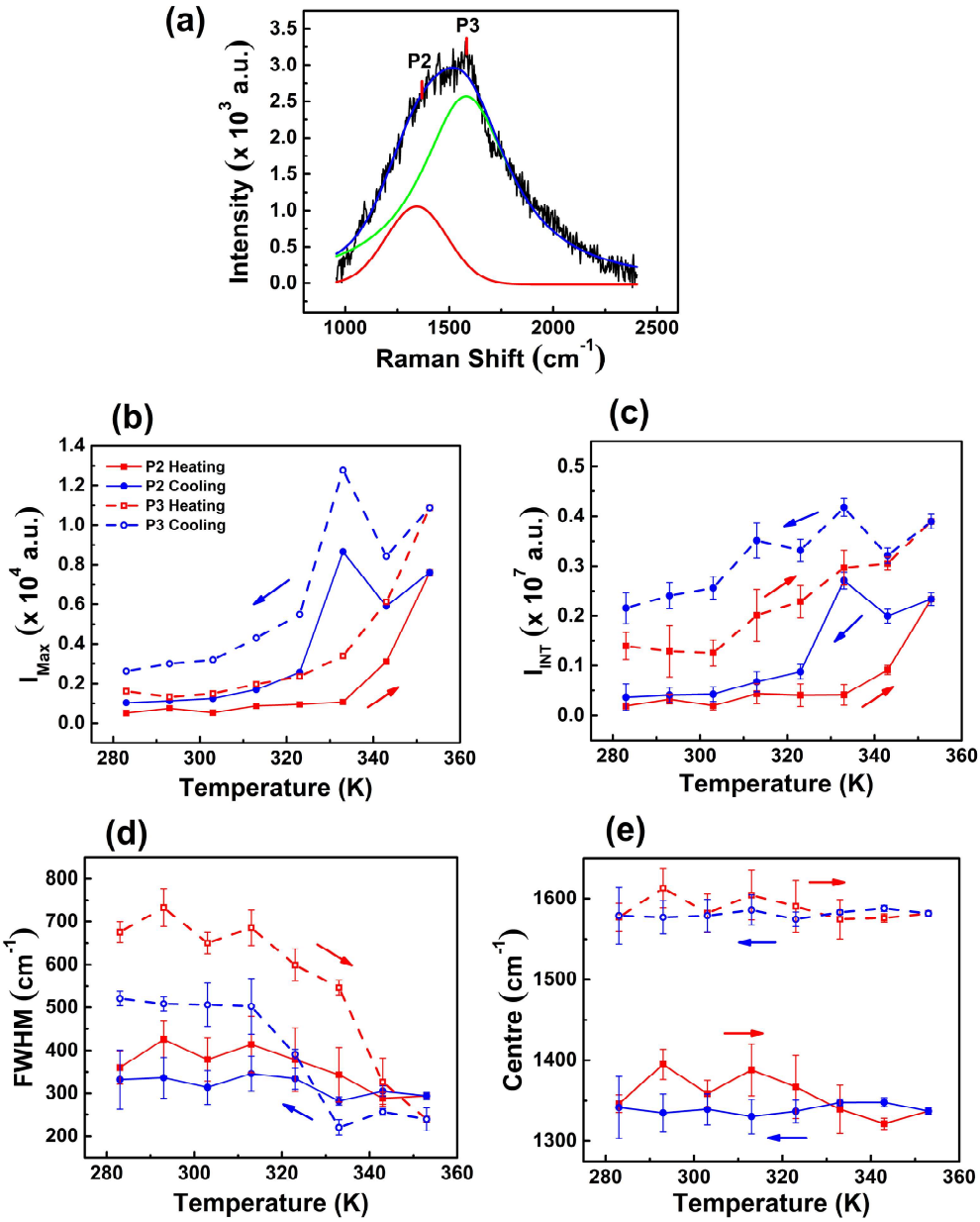

FIGURE 3.9: (a) The broad bands (peaks 2 and 3) appearing in the Raman spectrum of PVAc film, deconvoluted using Voigt function (Equation 3.3) at T = 313 K. Evolution of these peaks as a function of temperature for heating (red) and cooling (blue) cycles of ramp 1 (R1) for the peak parameters (b) peak height (I_{Max}), (c) peak area (I_{INT}), (d) FWHM and (e) peak center.

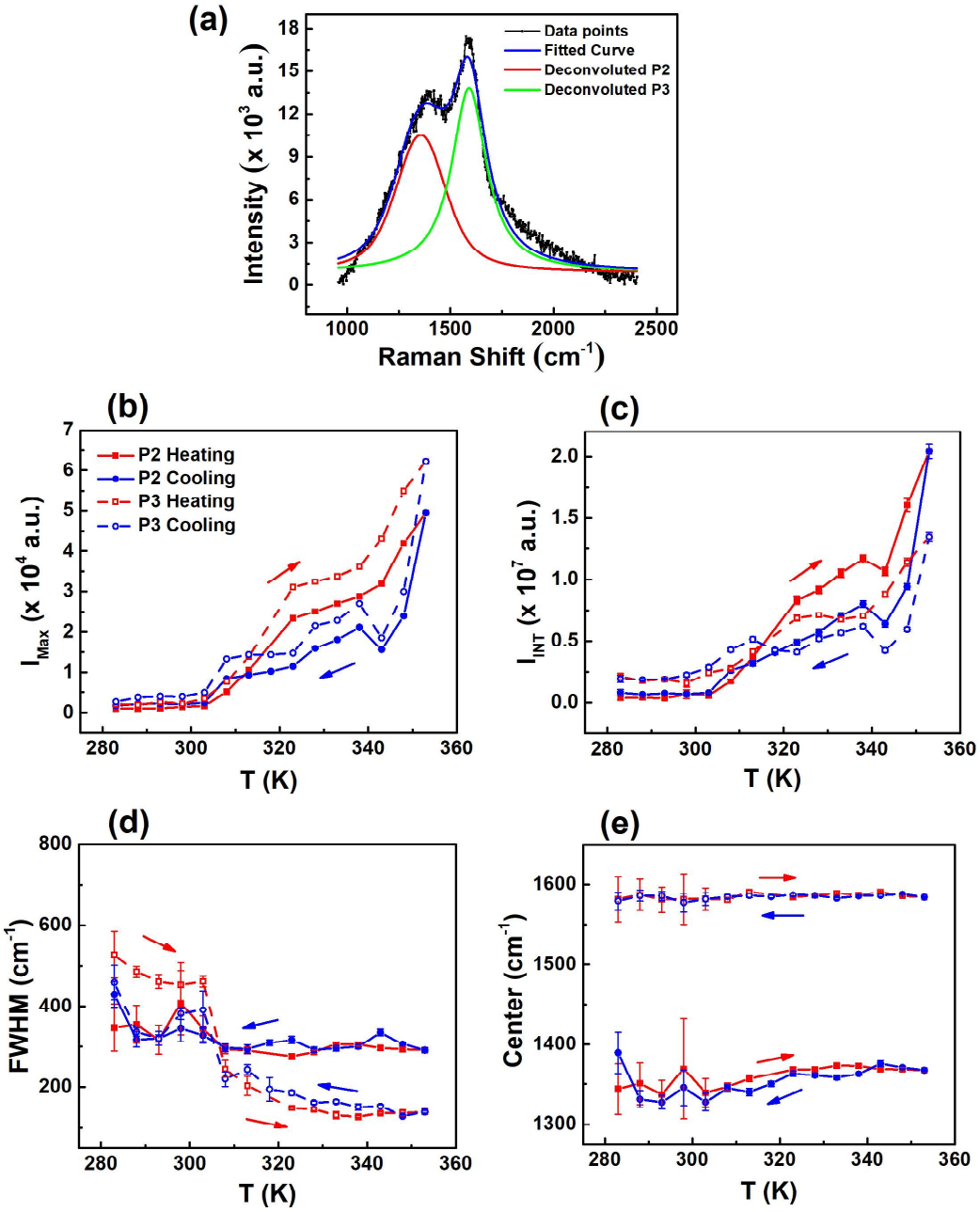

FIGURE 3.10: (a) The broad bands (peaks 2 and 3) appearing in the Raman spectrum of PVAc film, deconvoluted using Voigt function (Equation 3.3) at T = 313 K. Evolution of these peaks as a function of temperature for heating (red) and cooling (blue) cycles of ramp 2 (R2) for the peak parameters (b) peak height (I_{Max}), (c) peak area (I_{INT}), (d) FWHM and (e) peak center.

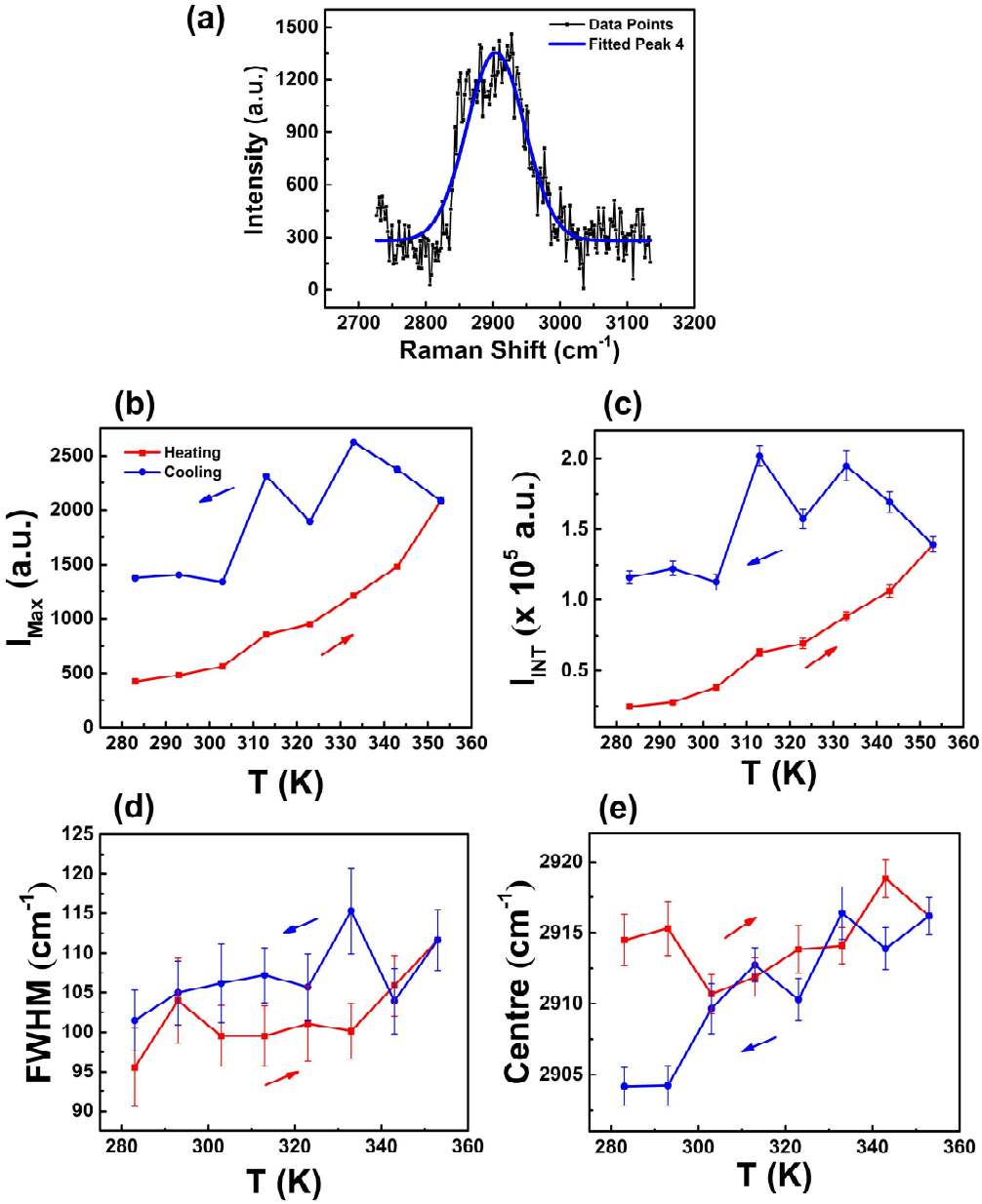

FIGURE 3.11: (a) C-H stretching mode (peak 4) appearing in the Raman spectrum of PVAc film, fitted using Lorentzian function (Equation 3.2) at T = 313 K. Effect of first temperature ramp (ramp 1) for heating (red) and cooling (blue) cycles for the peak parameters (b) peak height (I_{Max}), (c) peak area (I_{INT}), (d) FWHM and (e) peak center.

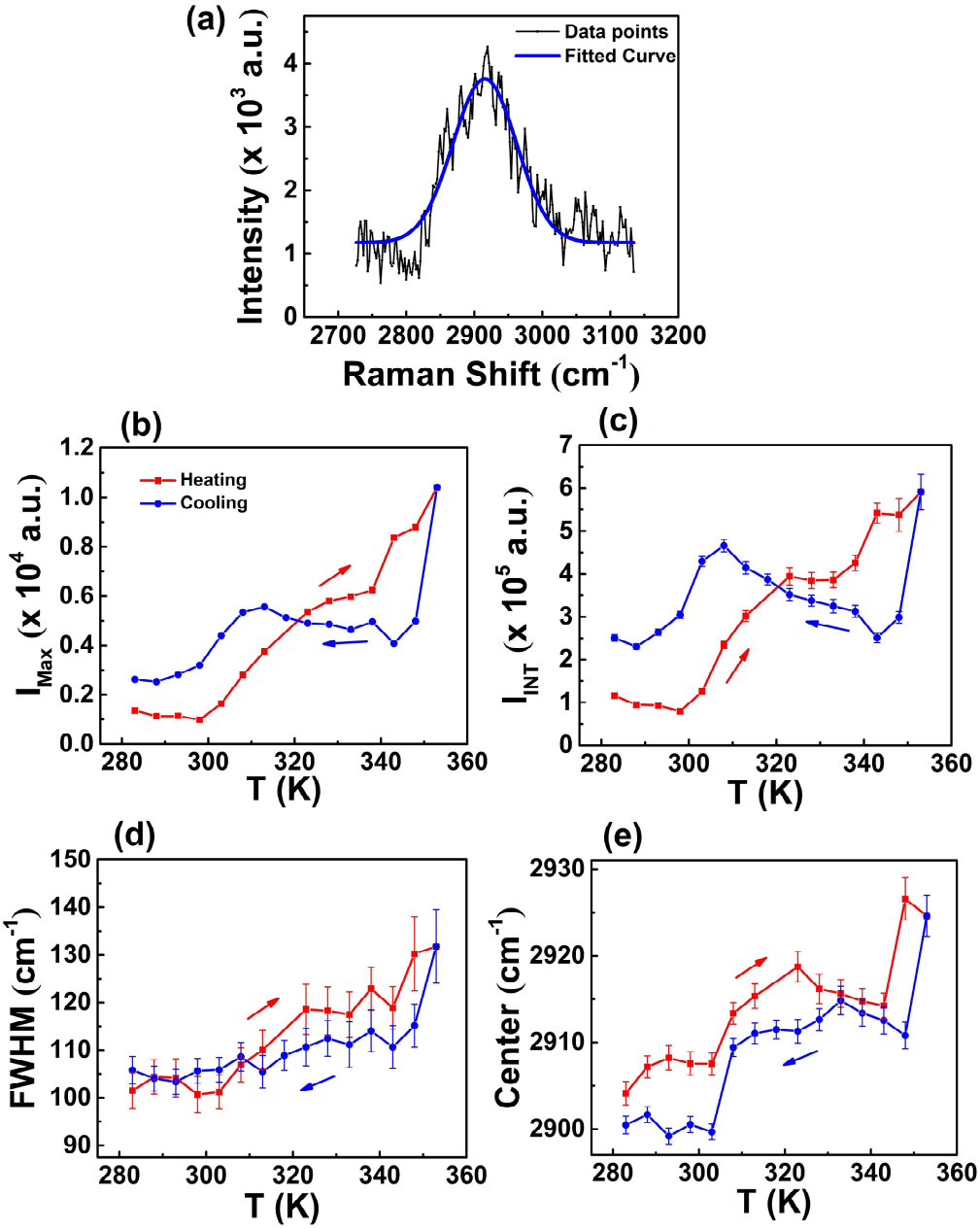

FIGURE 3.12: (a) C-H stretching mode (peak 4) appearing in the Raman spectrum of PVAc film, fitted using Lorentzian function (Equation 3.2) at T = 313 K. Effect of second temperature ramp (ramp 2) for heating (red) and cooling (blue) cycles for the peak parameters (b) peak height (I_{Max}), (c) peak area (I_{INT}), (d) FWHM and (e) peak center.

3.6.3 Analysis of hysteresis in Raman modes peak parameters

The response of unprocessed PVAc and PVAc film to the thermal ramp are very perceptible, but a common feature in both is the formation of hysteresis during the heating and cooling cycles of the thermal ramp. The area bounded by hysteresis gives an insight into the energy dissipated due to the thermal ramp applied. Since the thermal ramp is crossing the glass transition temperature (T_g), the hysteresis observed is most likely due to the variation in the conformational domains having domain boundaries forming energy barriers between the various states. The area bounded by the hysteresis is given by A^I_{INT}, shown in Figure 3.13 (a). As evident from the figure, the A^I_{INT} is higher in PVAc film as compared to unprocessed PVAc for both ramp 1 and ramp 2. This indicates that there is a higher number of configuration domains in PVAc film as compared to the unprocessed state which can be due to the disordered nature of PVAc film which makes it more vulnerable to driving it out of its equilibrium. Along with the A^I_{INT}, the difference between I_{INT} during heating and cooling cycles ($\triangle I_{INT}$) for PVAc film is also remarkably different and high from that of unprocessed PVAc.

Figure 3.13 (b) represents a comparison of the δI_{INT} of peak 7 (centered at 1736 cm^{-1}) of unprocessed PVAc which represents the C=O stretching mode present in the side branch of polymer and peak 2 of PVAc film (centered at 1350 cm^{-1}) which is a part of the broad band containing contributions from various vibrational modes present in the polymer. An interesting feature of $\triangle I_{INT}$ is that it increases with increasing T/T_g for PVAc film whereas it decreases with increasing T/T_g for unprocessed PVAc. The peaks representing the C-H stretching mode are also compared in Figure 3.13 (c) where peak 8 of unprocessed PVAc and peak 4 of PVAc film are compared. Here, the $\triangle I_{INT}$ for both unprocessed and film state of PVAc, increases with increasing T/T_g till it reaches a maximum at T/T_g = 1, after which the unprocessed PVAc starts decreasing continuously with increasing T/T_g but the PVAc film reaches a minimum at T/T_g = 1.05 and again starts increasing. A non-monotonic behavior is found in $\triangle I_{INT}$ of PVAc film, as a function of T/T_g.

The larger the hysteresis, the more the number of configurational domains and the higher the $\triangle I_{INT}$. The behavior of $\triangle I_{INT}$ of PVAc film represents a heterogeneous response of the Raman modes as a function of thermal cycling.

Not only in the C-H stretching mode but also in several other modes as depicted in Figure 3.13 (b), the variation of $\triangle I_{INT}$ for PVAc film resembles the heterogeneous character of the contributing Raman modes. The hysteresis observed in Raman mode intensities during temperature cycling thus illustrates the presence of conformational domains or clusters as suggested by the RFOT theory. In unprocessed PVAc, the $\triangle I_{INT}$ changes uniformly for both the Raman modes presented which indicates a smaller number of heterogeneities. According to RFOT, the glassy dynamics are slow and heterogeneous with various regions of variable conformational relaxations known as configurational mosaics. The energy barrier of these configurations around T_g is found to be $\sqrt{k_B T_g \delta C_p}$ = 365 J for PVAc [38], where $\triangle C_p$ is the variation in specific heat between the equilibrium state and near the glass transition temperature ($\triangle C_p$ = 12.4 cal mol^{-1}) for PVAc [15].

3.7 Effect of thermal quench

The thermal relaxations of PVAc were also studied by applying a thermal quench passing through T_g for both unprocessed PVAc and PVAc film. The thermal quench applied is illustrated in Figure 3.1 (b). The effect of thermal cycling is determined by studying the variation in the Raman peak parameters as a function of waiting time after quench (t_w).

3.7.1 Unprocessed PVAc

The thermal ramp applied to the polymer is carried out at two different quench rates: 60 °C/min and 100 °C/min. Figure 3.14 represents the Raman spectrum of unprocessed PVAc as a function of t_w for 60 °C/min (blue) and 100 °C/min (orange) to study the effect of quench rate on the thermal relaxation behavior. It is observed that the Raman spectrum is more intense for the quench rate 100 °C with slightly broader peaks. Similar to the thermal ramp, for the thermal quench of unprocessed PVAc, three peaks are chosen which can give an insight into the overall behavior of the polymer. The chosen peaks are: peak 2 centered at 1127 cm^{-1}, representing the C-C stretching modes present in the main chain of the polymer; peak 7 centered at 1735 cm^{-1} representing the C=O stretching modes present in the side branch of the polymer and peak 8 centered at 2940

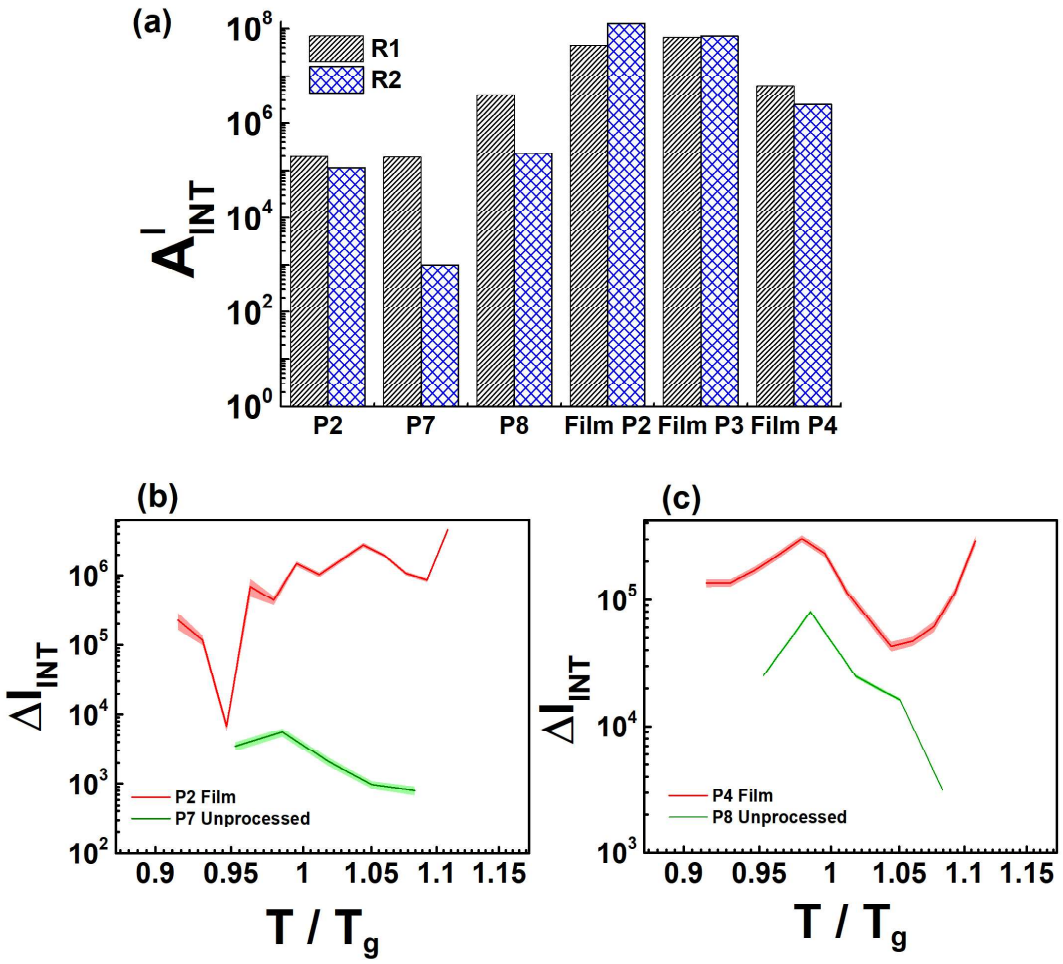

FIGURE 3.13: (a) The area covered by the hysteresis loop for unprocessed PVAc and PVAc film due to the thermal ramp cycle, R1 = ramp 1 and R2 = ramp 2. (b) The change in the area under the peak I_{INT} during the heating and cooling cycle represented as $\triangle I_{INT}$ vs T/T_g for peak 2 of PVAc film and peak 7 of unprocessed PVAc. (c) The change in the area under the peak I_{INT} during the heating and cooling cycle represented as $\triangle I_{INT}$ vs T/T_g for peak 4 of PVAc film and peak 8 of unprocessed PVAc.

cm^{-1} representing the C-H stretching mode present in both the main chain and side branch of the polymer.

The C-C stretching mode for unprocessed PVAc is shown in Figure 3.15 (a). For both the quench rates, the maximum peak intensity (I_{Max}) shows an increasing/decreasing behavior as a function of t_w as shown in Figure 3.15 (b). For 60 °C/min quench rate, the I_{Max} decreases with increasing t_w up to 20 minutes, after which it starts increasing and for 100 °C/min the minima are observed after 35 minutes of quench. The I_{INT} also shows a response similar to I_{Max} but the variation in I_{INT} is more discontinuous (Figure 3.15 (c)). The I_{Max} and I_{INT} for peak 2 are observed to be higher for 100 °C/min as compared to 60 °C /min. The FWHM shows a slight decrease of 25 cm^{-1} during 60 °C/min quench rate up to 20 minutes, after 20 minutes, the FWHM shows a fluctuating response (Figure 3.15 (d)). For 100 °C/min quench rate, the FWHM shows a negligible change with random fluctuations with increasing t_w. The peak center for peak 2 fluctuates as a function of t_w with larger fluctuations for 60 °C/min quench rate.

The effect of thermal quench on peak 7 representing C=O stretching mode is shown in Figure 3.16. The I_{Max} and I_{INT} for peak 7 show a fluctuating behavior with random increase and decrease in their magnitudes as shown in Figure 3.16 (b) and (c) respectively for I_{Max} and I_{INT}. It is observed that the I_{Max} and I_{INT} for 100 °C/min are higher than that of 60 °C/min. The FWHM and peak center on the other hand are the same for both the quench rates and they are also found to fluctuate with increasing t_w. The peak FWHM is found to fluctuate withing $\pm$ 1 cm^{-1} (Figure 3.16) and peak center fluctuates within $\pm$ 0.5 cm^{-1} (Figure 3.16 (e)).

The effect of thermal quench on peak 8 representing C-H stretching mode is shown in Figure 3.17. The response to thermal quench for peak 8 is similar to that of peak 2 and peak 7 where the I_{Max} and I_{INT} show a fluctuating behavior with random increase and decrease in their magnitudes as shown in Figure 3.17 (b) and (c) respectively for I_{Max} and I_{INT}. It is observed that the I_{Max} and I_{INT} for 100 °C/min are higher than that of 60 °C/min. The FWHM and peak center on the other hand are the same for both the quench rates and they are also found to fluctuate with increasing t_w. The peak FWHM fluctuates withing $\pm$ 0.5 cm^{-1} (Figure 3.17) and peak center fluctuates within $\pm$ 0.3 cm^{-1} (Figure 3.17 (e)).

A very common factor observed in the response of peak parameters as a function of t_w after quench for all the peaks in unprocessed PVAc is that the

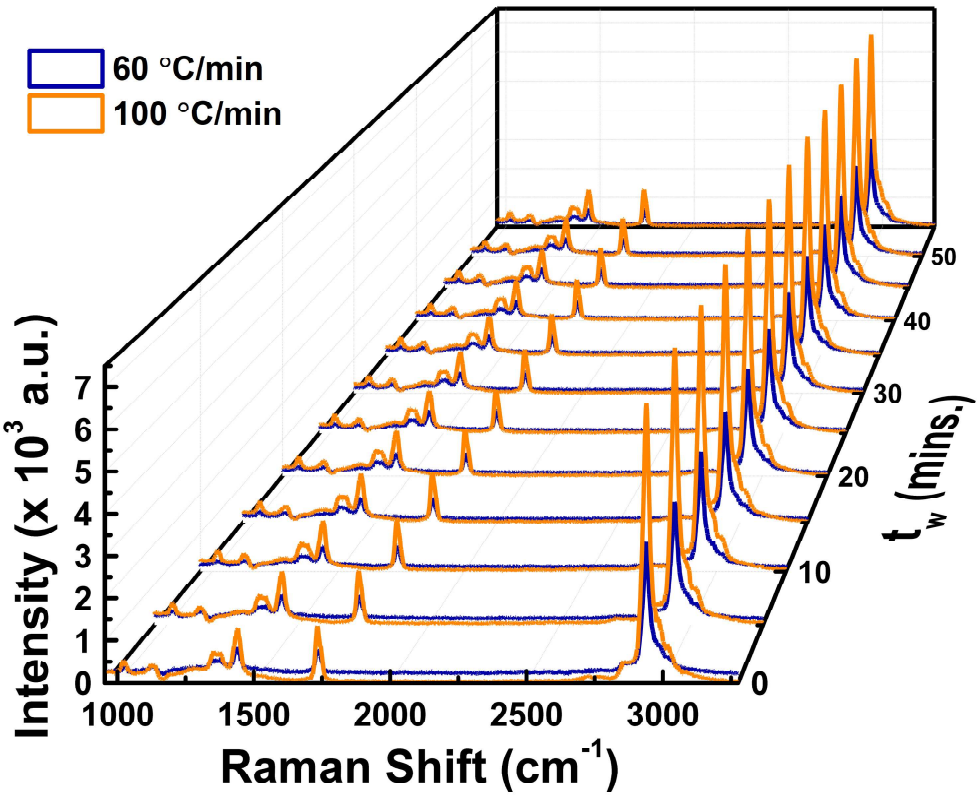

FIGURE 3.14: Time evolution of the Raman spectrum of unprocessed PVAc as a function of waiting time after quench (t_w) for two quench rates 60 °C/min (blue) and 100 °C/min (orange).

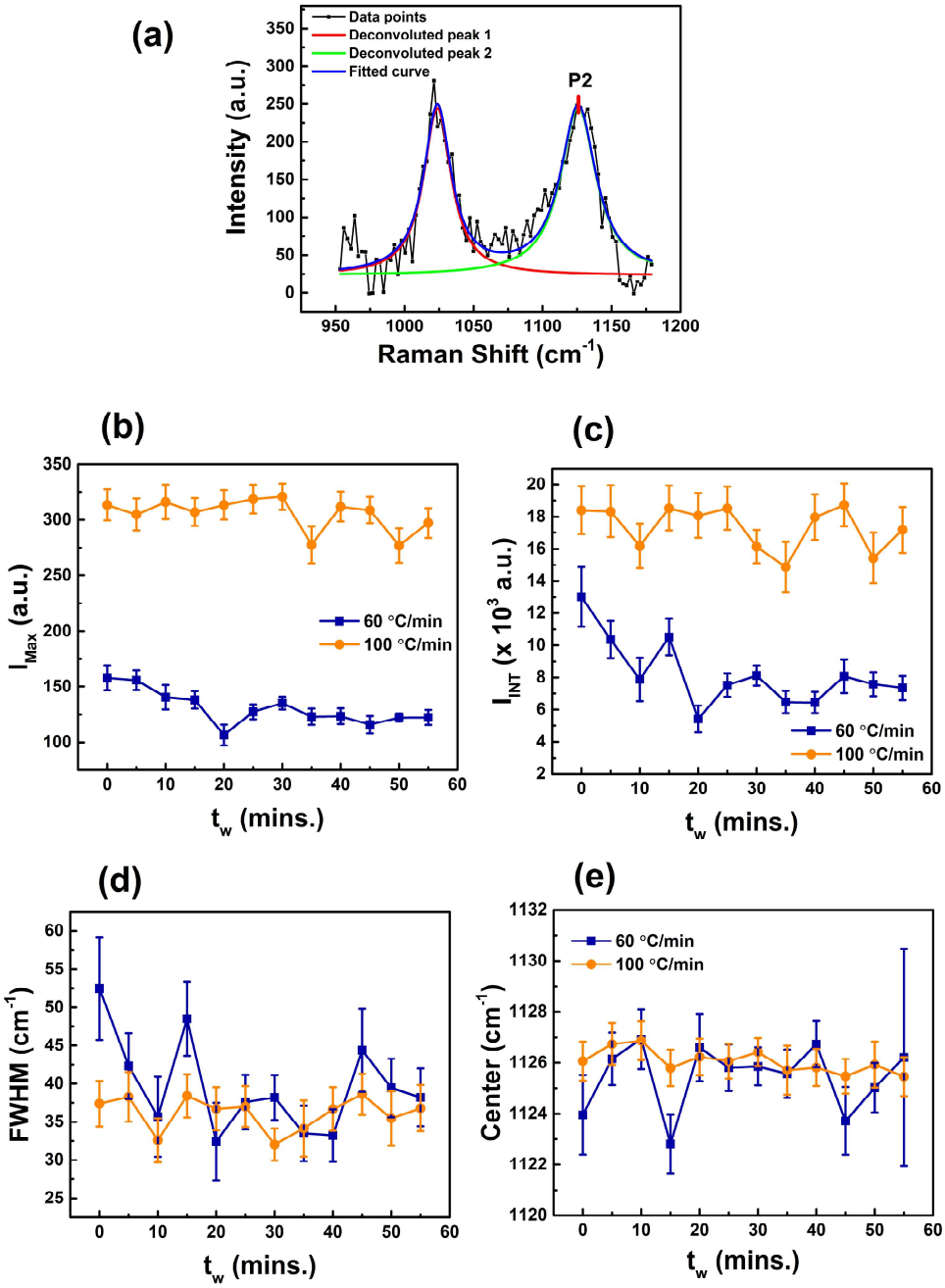

FIGURE 3.15: (a) C-C stretching peak (peak 2) of unprocessed PVAc fitted with Lorentzian function (Equation 3.2) which contributes to the side branch of the polymer. Time evolution of the peak fit parameters (b) peak height (I_{Max}), (c) peak area (I_{INT}), (d) FWHM, and (e) peak center as a function of waiting time after quench (t_w) for two quench rates 60 °C/min (blue) and 100 °C/min (orange)

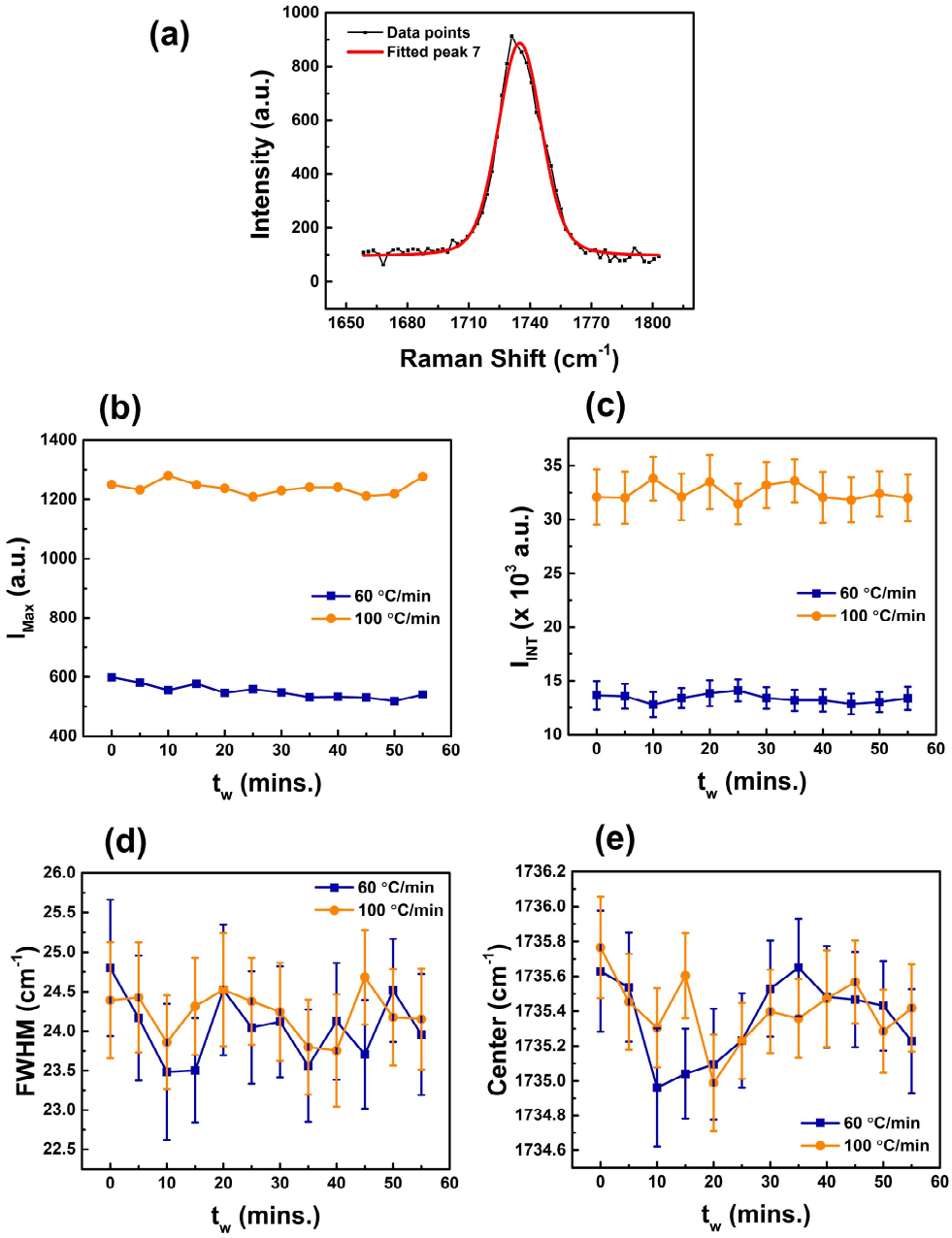

FIGURE 3.16: (a) C=O stretching peak (peak 7) of unprocessed PVAc fitted with Lorentzian function (Equation 3.2) which contributes to the side branch of the polymer. Time evolution of the peak fit parameters (b) peak height (I_{Max}), (c) peak area (I_{INT}), (d) FWHM, and (e) peak center as a function of waiting time after quench (t_w) for two quench rates 60 °C/min (blue) and 100 °C/min (orange).

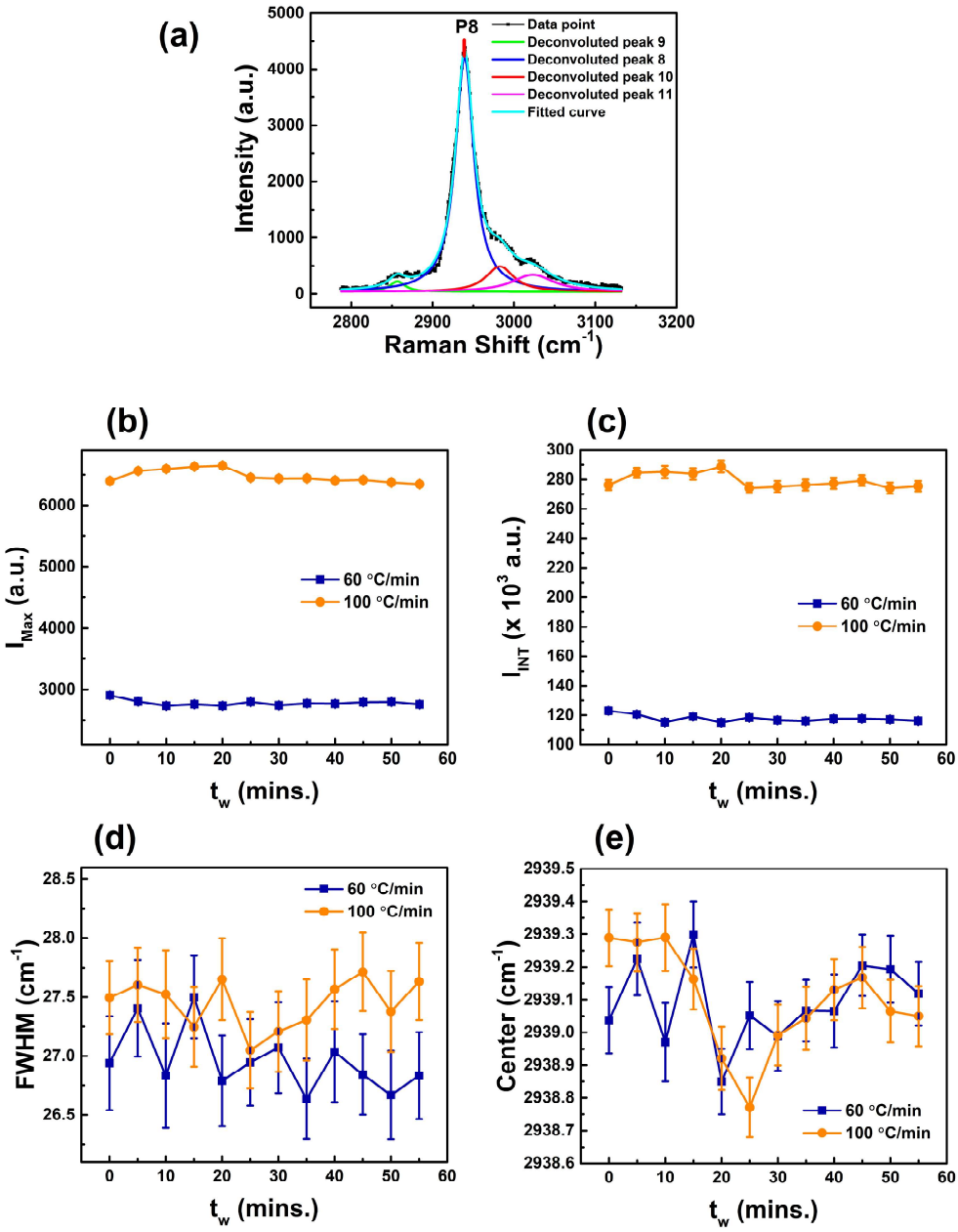

FIGURE 3.17: (a) C-H stretching peak (peak 8) of unprocessed PVAc fitted with Lorentzian function (Equation 3.2) which contributes to the side branch of the polymer. Time evolution of the peak fit parameters (b) peak height (I_{Max}), (c) peak area (I_{INT}), (d) FWHM, and (e) peak center as a function of waiting time after quench (t_w) for two quench rates 60 °C/min (blue) and 100 °C/min (orange)

faster quench rate (i.e. 100 °C/min) has a higher I_{Max} and I_{INT}. Increase in values of I_{Max} and I_{INT} is a signature of an increasing concentration of contributing molecules of the respective vibrational mode. This indicates that for faster quench rates there are more number of molecules excited which are contributing to the Raman spectrum which suggests that a faster quench rate can drive the unprocessed PVAc out of its equilibrium conditions.

3.7.2 PVAc film

The effect of thermal quench on the Raman spectrum of PVAc film is shown in Figure 3.18. Since the film state of PVAc has a disordered character, the thermal quench passing through the T_g is able to drive the system in its glassy state. In Figure 3.18, the blue curves represent the Raman spectrum of PVAc film as a function of t_w after quenching at a rate of 60 °C/min and the orange curve represents the Raman spectrum of PVAc film as a function of t_w after quenching at a rate of 100 °C/min. It is evident from Figure 3.18 that the quench rate of 60 °C/min has a higher effect on the Raman spectrum of PVAc film. To get a deeper insight into the thermal response of PVAc film, the three peaks appearing in the Raman spectrum of PVAc film were critically analyzed by studying the variations in peak fit parameters as a function of t_w.

The peak 2 deconvoluted from the broad Raman band in the Raman spectrum of PVAc film is shown in Figure 3.19 (a) which contains contributions from several vibrational modes appearing in the main chain as well as the side branch of the polymer. For 60 °C/min quench rate, the time evolution of I_{Max} (Figure 3.19 (b)) and I_{INT} (Figure 3.19 (c)) as a function of t_w show a continuous increasing behavior with increasing time with a maximum at 35 minutes after which there is a slight decrease with increasing t_w. For 100 °C/min quench rate, the I_{Max} and I_{INT} show a continuous increase as a function of t_w. It can be observed that the I_{Max} and I_{INT} for 60 °C/min have higher magnitude as compared to 100 °C/min, this behavior is opposite to the response to thermal quench of unprocessed PVAc. The FWHM for peak 2 of PVAc film shows a decreasing behavior as a function of t_w for both quench rates (Figure 3.19 (d)) whereas the peak center shows an increase towards higher wavenumbers with increasing t_w for both quench rates (Figure 3.19 (e)).

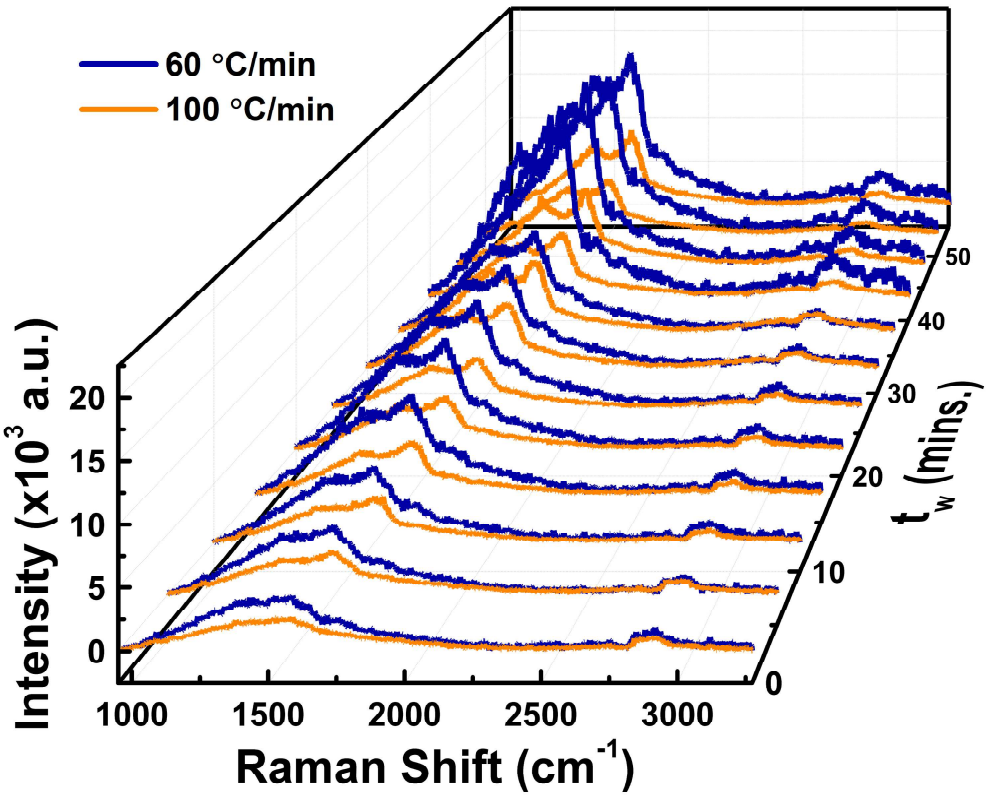

FIGURE 3.18: Time evolution of the Raman spectrum of PVAc film as a function of waiting time after quench (t_w) for two quench rates - 60 °C/min (blue) and 100 °C/min (orange).

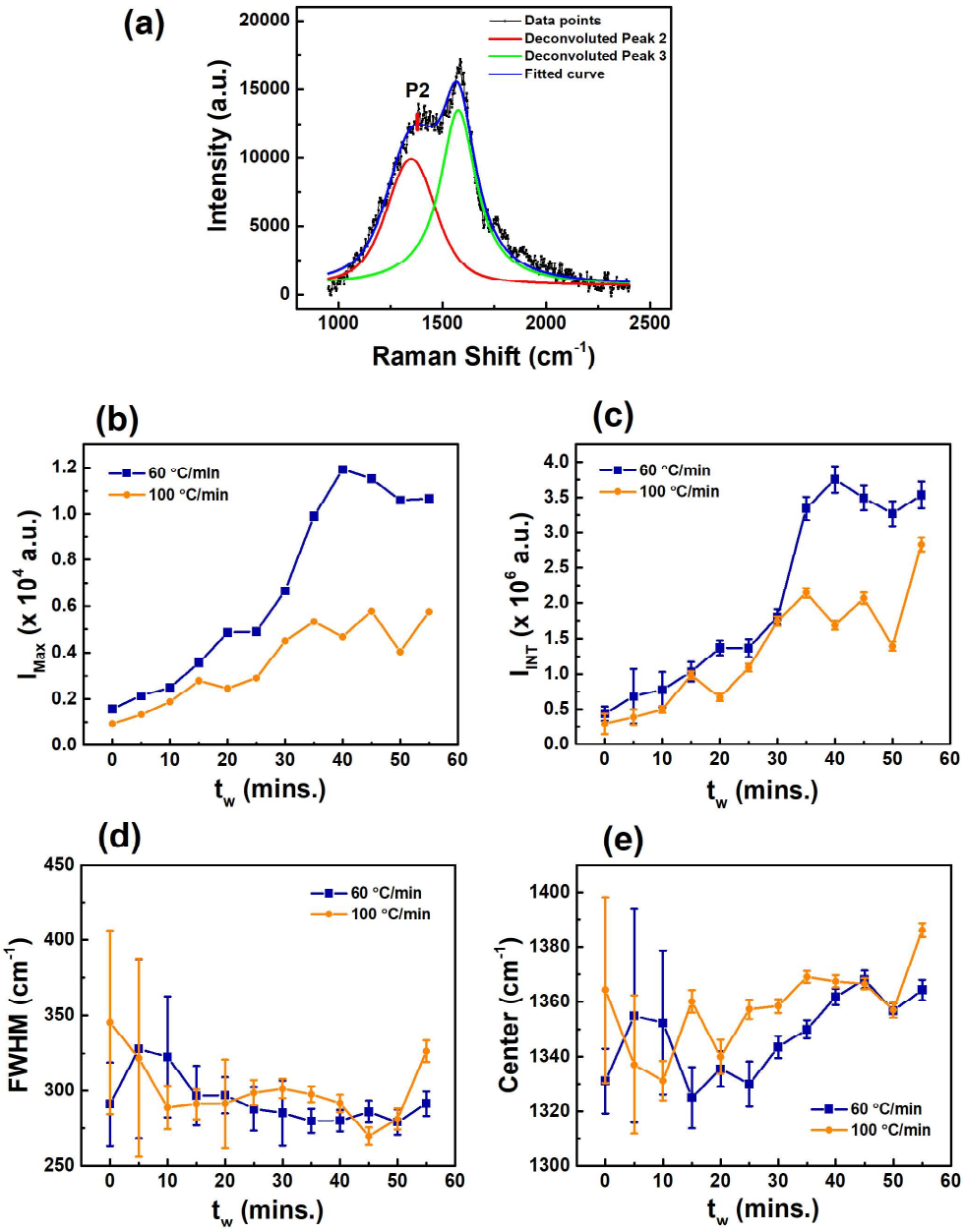

FIGURE 3.19: (a) Peak 2 of the Raman band appearing in the Raman spectrum of PVAc film, fitted using Voigt function (Equation 3.3). Time evolution after quench for two quench rates - 60 °C/min (blue) and 100 °C/min (orange) of the peak fit parameters (b) peak height (I_{Max}), (c) peak area (I_{INT}), (d) FWHM and (e) peak center.

The peak 3 deconvoluted from the broad Raman band in the Raman spectrum of PVAc film is shown in Figure 3.20 (a) which contains contributions from several vibrational modes appearing in the main chain as well as the side branch of the polymer. For 60 °C/min quench rate, the time evolution of I_{Max} (Figure 3.20 (b)) and I_{INT} (Figure 3.20 (c)) as a function of t_w shows a continuous increasing behavior with increasing time with a maximum at 35 minutes after which there is a slight decrease with increasing t_w. For 100 °C/min quench rate, the I_{Max} shows a continuous increase as a function of t_w and I_{INT} shows a decreasing character with t_w. Similar to peak 2 of PVAc film, the I_{Max} and I_{INT} for 60 °C/min have higher magnitude as compared to 100 °C/min. The FWHM for peak 2 of PVAc film shows a continuous decrease as a function of t_w for both quench rates (Figure 3.20 (d)) whereas the peak center increases to higher wavenumbers with increasing t_w for both quench rates (Figure 3.20 (e)).

The C-H stretching mode represented by peak 4 of PVAc film is shown in Figure 3.21 (a). The I_{Max} (Figure 3.21 (b)) and I_{INT} (Figure 3.21 (c)) for peak 4 after quenching at a rate of 60 °C/min show a behavior similar to peak 2 and peak 3 of PVAc film which increases with increasing t_w with a maximum at 40 minutes followed by a slight decrease. For quench rate 100°C/min, the I_{Max} and I_{INT} show a maximum at 35 minutes, after which it starts decreasing. The I_{Max} for peak 4 during 60 °C/min is slightly higher than I_{Max} during °C/min and the I_{INT} of peak 4 is almost the same during both quench rates. The FWHM of peak 4 shows an increasing character during both the quench rates with maxima at 35 minutes as shown in Figure 3.21 (d). After 35 minutes the FWHM is found to decrease with t_w. The peak center for peak 4 of PVAc film shows an increase towards higher wavenumbers with a maximum at 40 minutes after quenching with a rate of 60 °C/min and it decreases towards lower wavenumbers with a minimum at 35 minutes after quenching with a rate of 100 °C/min.

The fluctuations in the temporal evolution of the peak parameters for both unprocessed PVAc and PVAc film represent the variation in the molecular architecture of the polymer domains. The increasing I_{Max} is a representation of the increasing concentration of the contributing molecules to the Raman spectrum. The fluctuation in I_{Max} as observed in unprocessed PVAc and PVAc film indicates that there is a presence of heterogeneity in the contributing molecules. Another important factor in the determination of thermal response is the variation in FWHM where the increase in FWHM could be due to

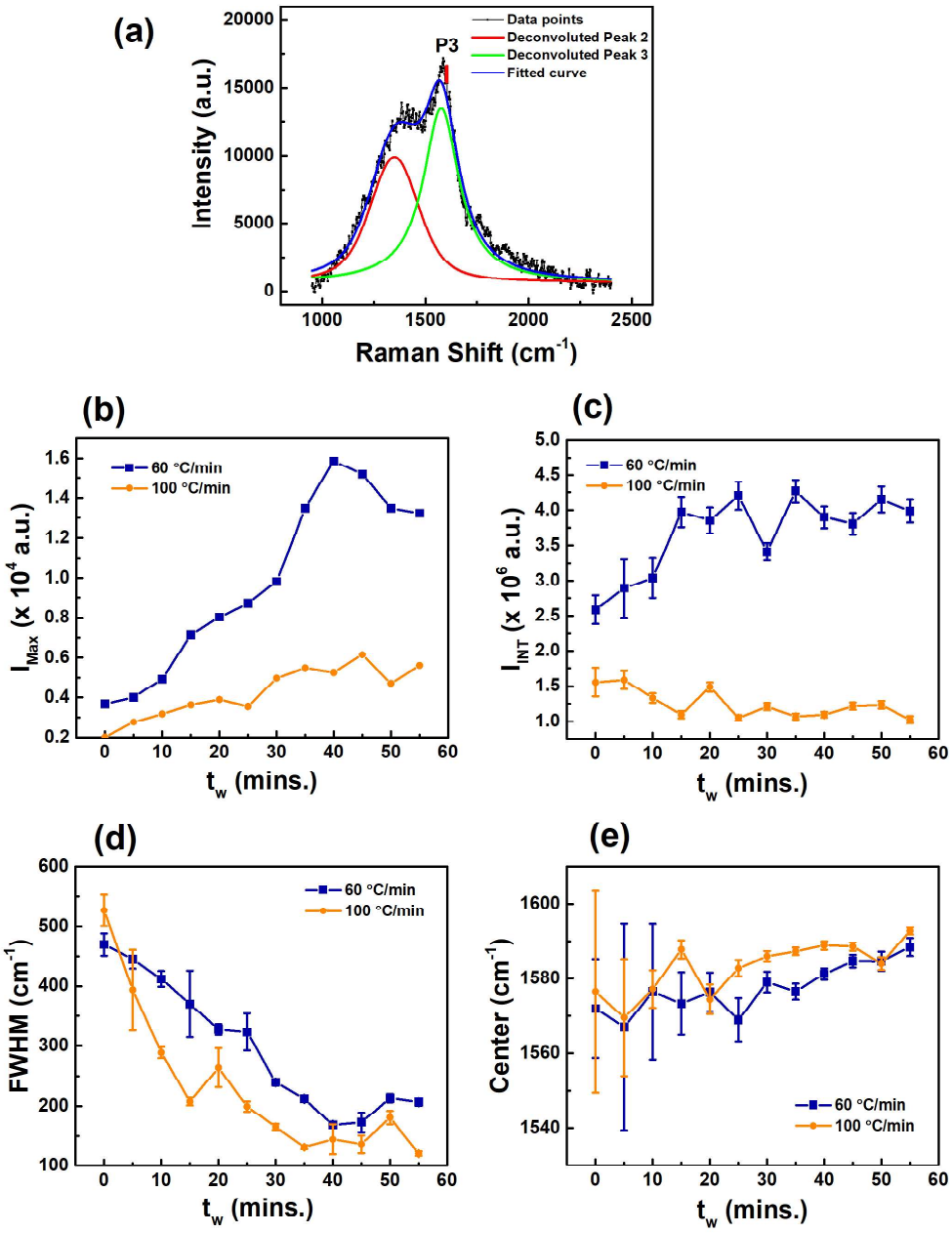

FIGURE 3.20: (a) Peak 3 of the Raman band appearing in the Raman spectrum of PVAc film, fitted using Voigt function (Equation 3.3). Time evolution after quench for two quench rates - 60 °C/min (blue) and 100 °C/min (orange) of the peak fit parameters (b) peak height (I_{Max}), (c) peak area (I_{INT}), (d) FWHM and (e) peak center.

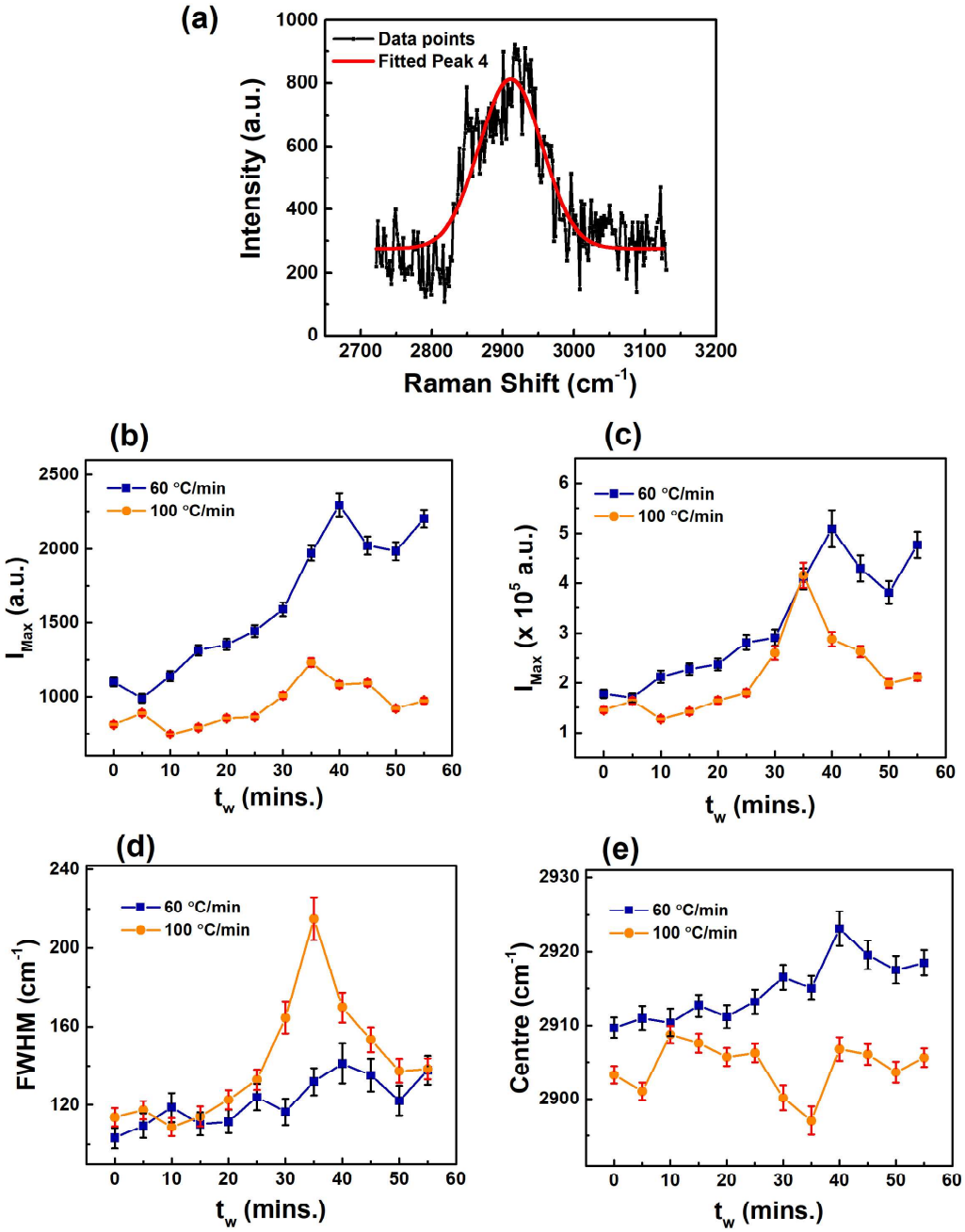

FIGURE 3.21: (a) C-H stretching mode (peak 4) appearing in the Raman spectrum of PVAc film, fitted using Lorentzian function (Equation 3.2). Time evolution after quench for two quench rates - 60 °C/min (blue) and 100 °C/min (orange) of the peak fit parameters (b) peak height (I_{Max}), (c) peak area (I_{INT}), (d) FWHM and (e) peak center.

enhancement in molecular mobility within the polymer matrix. Peak broadening in the Raman spectrum represents higher mobile regions and the fluctuations in the Raman peak FWHM show a signature of heterogeneous regions of high and low mobility. This signature of Raman peak parameters represents the presence of heterogeneities at the molecular scale and Raman spectroscopy in this case has proved to be a useful tool to probe these heterogeneities. The existence of molecular mobility is due to the thermal relaxations introduced in the polymeric system due to the thermal perturbations applied.

3.8 Thermal relaxation of Raman modes

When the temperature of a polymer is increased, several thermally activated molecular motions and conformational changes are introduced and the system is said to be relaxing. The relaxation process in polymers is governed by molecular motions which can be a cooperative motion of large chains of the polymer or can be due to the local motion of small parts of the polymer. The temperature ramp cycle provides enough thermal energy for the polymeric molecules to move along each other, it creates several variations in the inter-molecular and intra-molecular conformation and orientation of the polymer. This motion induces several vibrational and rotational transitions inside the molecule which can be visualized in the Raman spectrum. The variation in peak height, area, FWHM, and center of the Raman peaks due to the thermal cycles indicate the presence of a thermally activated relaxation process.

The relaxation process can be categorized into α and β relaxation. The β relaxation is the relaxation of local monomeric units or can be known as structural relaxation. When the molecules are trapped in a cage-like potential well they require some amount of energy to come out and relax, the thermal cycle provides this energy to the molecules and the molecule starts relaxing. This minimum amount of energy required by the molecule to relax is known as the activation energy denoted by E_a. The β relaxation mainly follows the Arrhenius equation which is given by:

$$\tau_\alpha = \tau_0 \exp \frac{E_a}{k_B T} \tag{3.4}$$

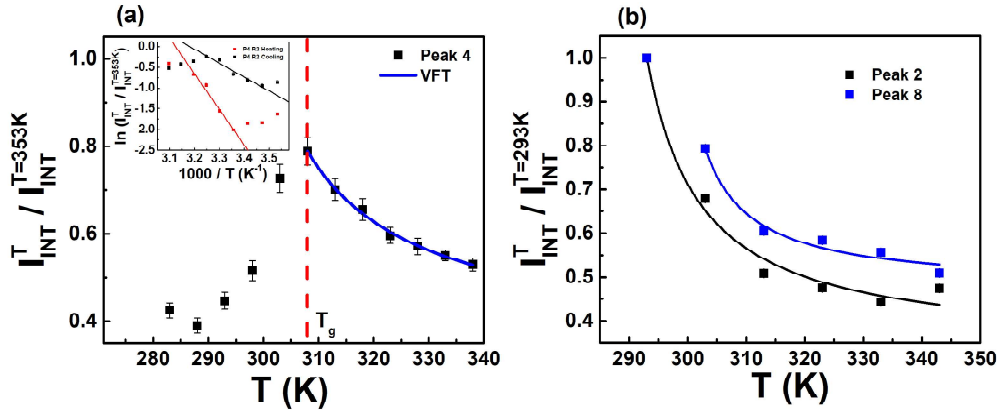

FIGURE 3.22: (a) The temperature dependence of normalized I_{INT} for peak 4 of PVAc film follows a VFT relation after T_g (shown by red dashed line and an Arrhenius equation before T_g). (b) The temperature dependence of normalized I_{INT} for peak 2 and peak 8 of unprocessed PVAc fitted with VFT relation.

The α relaxation attributes to the macro-molecular changes in the polymer which includes large segmental motion of the polymer chains on approaching T_g. For fragile glass formers wherein the relaxation is governed by α relaxations, the effective activation energy which is determined by the Arrhenius behavior increases with temperature and this behavior is known as non-Arrhenius behavior which is represented by the Vogel Fulcher Tamann (VFT) Equation given by:

$$\tau_\alpha = \tau_0 \exp \frac{DT_0}{T - T_0} \tag{3.5}$$

The VFT equation suggests that the relaxation time diverges from Arrhenius behavior at a finite temperature T_0 known as fictive temperature which represents the presence of a phase transition and D is the fragility index where smaller D indicates that the glass is more fragile[11, 39].

To determine the relaxations present inside unprocessed PVAc and PVAc film, the peak area (I_{INT}) for the peaks is plotted as a function of temperature during the cooling cycle of the second ramp; since the first ramp was mainly performed to anneal the polymer so it is not considered for further analysis. Figure 3.22 (a) represents the normalized I_{INT} of peak 4 in PVAc film as a function of temperature. The I_{INT} is normalized by the maximum I_{INT} which is occurring at T = 353 K, and the normalized I_{INT} is denoted by I^T_{INT}. The thermal

response of PVAc film can be divided into three regimes representing the characteristic relaxations. It can be observed that the I_{INT} reaches a maximum at a temperature near T_g and then decreases with increasing temperature. Since the relaxations have their characteristic temperature upto which the relaxation behavior can be observed so the regimes were fitted to Arrhenius (Equation 3.4) and VFT equation (Equation 3.5) and it is observed that as the temperature is cooled from 353 K to 313 K, there is an α relaxation regime given by VFT relation (Equation 3.5) which represents that the relaxation of the polymer chain is cooperative along the length of the polymer and when the temperature is decreased further, the relaxation dynamics experiences a transition from the cooperative dynamics to activated dynamics also known as β relaxation, which is represented in the form of Arrhenius relation (Equation 3.4). This transition from α to β relaxation is evident in peak 4 of PVAc film (Figure 3.22 (a)) and the point where this transition occurs is found to be near T_g of the polymer. The other two peaks present in the Raman spectrum of PVAc film are unable to distinguish between the α and β relaxation because these peaks involve contributions from a lot of vibrational and rotational modes present within the polymer.

It is evident from the above results that with decreasing temperature, the polymer chain relaxes with a macro-molecular segmental motion until the temperature reaches its T_g. Below T_g the dynamics become slower and a local motion of the monomeric molecules is observed. The β relaxation is a signature of the dynamic arrest which is observed on cooling below the T_g. The deviation towards the Arrhenius behavior on approaching T_g also indicates the increasing fragility of the polymer. This divergence of the dynamics on approaching the T_g is in agreement with the dielectric measurements in PVAc glass former where Arrhenius-type behavior is observed below T_g [40]. The results also support Yang's prediction based on energy landscapes that there is no divergence from the Arrhenius behavior below T_g [41].

In unprocessed PVAc, the peak area (I_{INT}) is plotted as a function of temperature for peak 2 from region 1 which represents C-C stretching vibrations in the main chain of the polymer, and peak 8 in region 3 which represents C-H asymmetric stretching vibrations in unprocessed PVAc. To determine the characteristic relaxation of different modes the I_{INT} as a function of temperature the I_{INT} for unprocessed PVAc is normalized with the maximum I_{INT} which

occurs at T = 293 K and is fitted with 3.4 and 3.5. It is observed that unlike PVAc film, the unprocessed PVAc only contains a single relaxation regime as shown in Figure 3.22 (b). The I_{INT} for unprocessed PVAc follows the VFT equation (3.5) which indicates the presence of α relaxations. Hence, in unprocessed PVAc, the thermal cycle is unable to provide energy for the monomers to relax instead the relaxation is mainly governed by the change in the long segmental motion of the polymer chains. The β relaxation regime which is prominently appearing in the PVAc film did not appear in the applied temperature range for unprocessed PVAc. The onset of β relaxation has shifted to a lower temperature in unprocessed PVAc as compared to PVAc film therefore we are able to capture only α relaxation regime in the unprocessed PVAc. The VFT fit of the peak area in unprocessed PVAc is shown in Figure 3.22(b). The fitting results are given in Table 3.2 for the Arrhenius fitting and in Table 3.3 for VFT fitting respectively.

For the C-H stretching mode of PVAc film, the thermal relaxations fit better to the Arrhenius equation (3.4) which shows a predominance of thermally activated relaxation process which is dominated by conformational changes with an activation energy of 27 $\pm$ 3 kJ/mol. During the heating cycle, the activation energy increases to 71 $\pm$ 6 kJ/mol which is more than double the energy during the cooling cycle but this behavior is dominant only up to 308 K. Similar results are obtained for peaks 2 and 3 of PVAc film which are given in Table 3.2 but the crossover from the thermal relaxations is only observed in the C-H mode of PVAc film. The VFT fitting for the C-H stretching mode in PVAc film is found beyond 308 K and the fragility of the film is determined from the film which is found to be 0.087 $\pm$ 0.026. In unprocessed PVAc, both C-C as well as C-H modes are fitting well with a VFT function (3.5) as shown in Figure 3.22(b), and the fragility index for the modes is found to be D_{CC} =0.058 $\pm$ 0.027 and D_{CH} = 0.01793 $\pm$ 0.01197 respectively. From the fragility index, one can interpret that the unprocessed state of PVAc is more fragile as compared to the film state.

It is evident from Figure 3.22 that the relaxations in unprocessed PVAc are non-Arrhenius and the molecular motion is dominated by the macro-molecular chain motion of the polymer. On the other hand, a crossover from non-Arrhenius to Arrhenius behavior is observed in the PVAc film. A localized motion is observed prominently in the film state of PVAc below T_g. Significant differences are observed in the relaxations of the unprocessed and film state of

TABLE 3.2: Calculation of activation energy from the Arrhenius fits (Equation 3.4) of the integrated peak intensities (I_{INT}^{T}) of Raman peaks 2, 3 and 4 of PVAc film.

Peak No.	Intercept (ln I_o)	Slope	E_a (KJ/mol)
Ramp 2 Heating P4	26 ± 2	8.5 ± 0.8	71 ± 6
Ramp 2 Cooling P4	10 ± 1	3.3 ± 0.3	27 ± 3
Ramp 2 Heating P2	41 ± 4	13 ± 1	112 ± 11
Ramp 2 Cooling P2	21 ± 5	7 ± 1	61 ± 13
Ramp 2 Heating P3	20 ± 3	6.7 ± 0.9	55 ± 7
Ramp 2 Cooling P3	14 ± 2	4.9 ± 0.8	41 ± 6

TABLE 3.3: Fitting results of integrated peak intensities as a function of temperature ($I_{INT}^{T=293K}$) fitted with VFT equation (Equation 3.5) during cooling cycle of thermal ramp 2.

Peak No.	a	D	T_0 (K)
2. (Bulk PVAc)	0.46 ± 0.09	0.007 ± 0.01	300 ± 1
7. (Bulk PVAc)	0.51 ± 0.03	0.006 ± 0.005	299.9 ± 0.7
8.(Bulk PVAc)	0.67 ± 0.03	0.002 ± 0.002	301 ± 0.3
4. (PVAc Film)	0.35 ± 0.02	0.08 ± 0.02	277 ± 5

PVAc. A similar study on the bulk and film state of polystyrene using optical photobleaching technique [22] has reported the deviation from the bulk behavior for the glassy state of the polymer film. Many other evidences of the transition between Arrhenius and VFT-like dynamics have been reported below and above T_g.

3.9 Summary

The present study reveals a clear distinction observed in the Raman mode relaxations of PVAc in the film state and unprocessed PVAc. Although the PVAc film is reasonably thick and its glass transition temperature is hardly different from the unprocessed PVAc, resulting in much lower interfacial interactions and confinement effects than observed in the nanometer-scale polymer films, thermal cycling through T_g leads to stronger hysteresis in the film compared to the unprocessed state, implying enhancement in the number of configurational mosaics (in the context of the RFOT) leading to larger interfacial energy dissipations in the film state. A large number of closely spaced conformational

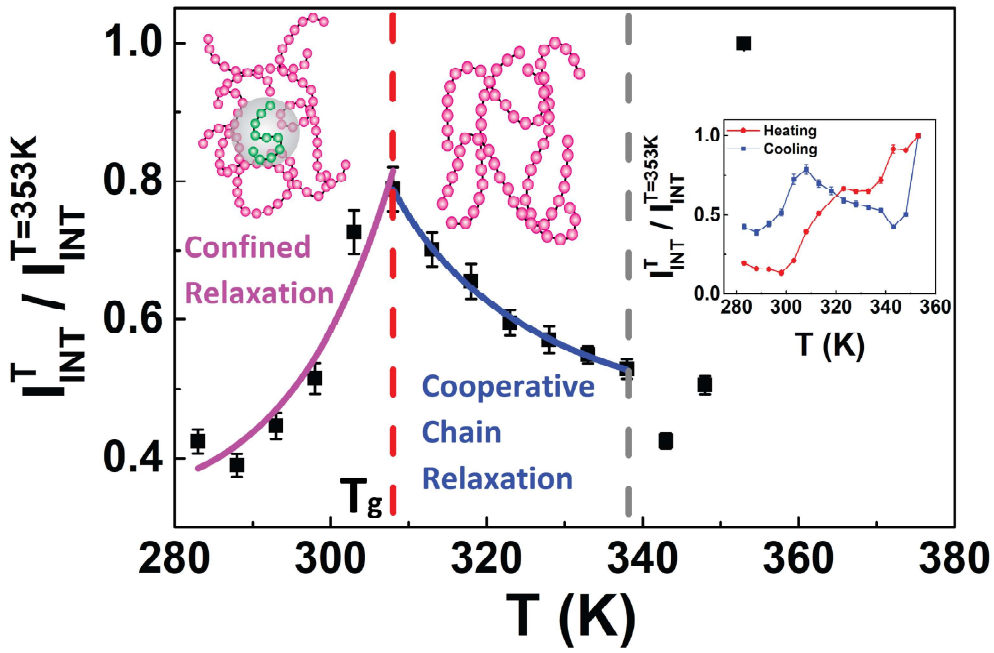

FIGURE 3.23: Schematic representation of the thermal relaxations observed in PVAc film during the thermal ramp passing through T_g. A clear transition from the cooperative segmental dynamics to confined caging dynamics is observed on going below T_g.

modes is also reflected in the broadening of the Raman bands in the film. In the case of unprocessed PVAc, where the Raman modes of the polymer are discerned, thermal cycling through T_g clearly shows the coupling between the main chain C-C modes with the side chain C=O, CH_2 modes and the C-H stretching modes, which is evident from trends in the peak area for all the modes also shown in Figure 3.23 and a strong correlation is also observed in these modes which will be discussed in next chapter. Neutron scattering experiments with PVAc have seen this coupling between the main chain and side chain relaxations, or intra-chain cooperativity [42]. These neutron scattering experiments also observe strong inter-chain correlations in PVAc. Signatures of enhanced correlations due to dynamic heterogeneities in the glassy state have been observed in computer simulations of athermal systems [43]. Strong support for growing correlation length scale and shapes of cooperatively rearranging regions as predicted by RFOT is observed in video microscopy experiments in colloidal glass formers [44]. In the present study, we have focussed on the molecular relaxations of a polymer glass in the context of a purely thermodynamic framework as supported by the RFOT. However, a study of these glass formers in the context of the dynamic facilitation theory, which takes into account the concerted structural relaxations arising as a result of the propagation of localized defects would be interesting, and possible by single molecule studies of structural relaxations in polymer glasses, which can give more insights into the structural origins of the cooperative heterogeneous dynamics in polymer glasses.

Refernces

[1] Qiang Matthew Zhang and Michael J Serpe. Synthesis, characterization, and antibacterial properties of a hydroxyapatite adhesive block copolymer. *Macromolecules*, 47(22):8018–8025, 2014.

[2] Sreyan Ghosh, Riya Mukherjee, Debajyoti Basak, and Jayanta Haldar. One-step curable, c ovalently immobilized coating for clinically relevant surfaces that can kill bacteria, fungi, and influenza virus. *ACS Applied Materials & Interfaces*, 12(25):27853–27865, 2020.

[3] Shuqi Wang, Yaming Wang, Yongchun Zou, Guoliang Chen, Jiahu Ouyang, Dechang Jia, and Yu Zhou. Scalable-manufactured superhydrophobic multilayer nanocomposite coating with mechanochemical robustness and high-temperature endurance. *ACS Applied Materials & Interfaces*, 12(31):35502–35512, 2020.

[4] Haibin Xu and Yixia Zhang. A review on conducting polymers and nanopolymer composite coatings for steel corrosion protection. *Coatings*, 9(12):807, 2019.

[5] Wenjing Hou, Yaoming Xiao, Gaoyi Han, and Jeng-Yu Lin. The applications of polymers in solar cells: A review. *Polymers*, 11(1):143, 2019.

[6] Min Kim, Silvia G Motti, Roberto Sorrentino, and Annamaria Petrozza. Enhanced solar cell stability by hygroscopic polymer passivation of metal halide perovskite thin film. *Energy & Environmental Science*, 11(9):2609–2619, 2018.

[7] Ahalya Gunasekaran, Andrea Sorrentino, Abdullah M Asiri, and Sambandam Anandan. Guar gum-based polymer gel electrolyte for dye-sensitized solar cell applications. *Solar Energy*, 208:160–165, 2020.

[8] Saumya R Mohapatra, Tohru Tsuruoka, Karthik Krishnan, Tsuyoshi Hasegawa, and Masakazu Aono. Effects of temperature and ambient pressure on the resistive switching behaviour of polymer-based atomic switches. *Journal of Materials Chemistry C*, 3(22):5715–5720, 2015.

[9] Christian Muller. On the glass transition of polymer semiconductors and its impact on polymer solar cell stability. *Chemistry of Materials*, 27(8):2740–2754, 2015.

[10] Liang Wang, Hong Zhang, Chaolei Wang, and Tingli Ma. Highly stable gel-state dye-sensitized solar cells based on high soluble polyvinyl acetate. *ACS Sustainable Chemistry & Engineering*, 1(2):205–208, 2013.

[11] Ludovic Berthier and Giulio Biroli. Theoretical perspective on the glass transition and amorphous materials. *Reviews of Modern Physics*, 83(2):587, 2011.

[12] Pablo G Debenedetti and Frank H Stillinger. Supercooled liquids and the glass transition. *Nature*, 410(6825):259–267, 2001.

[13] Koji Fukao and Yoshihisa Miyamoto. Slow dynamics near glass transitions in thin polymer films. *Physical Review E*, 64(1):011803, 2001.

[14] Ludovic Berthier, Giulio Biroli, Jean-Philippe Bouchaud, Luca Cipelletti, and Wim van Saarloos. *Dynamical heterogeneities in glasses, colloids, and granular media*, volume 150. OUP Oxford, 2011.

[15] Gerold Adam and Julian H Gibbs. On the temperature dependence of cooperative relaxation properties in glass-forming liquids. *The journal of chemical physics*, 43(1):139–146, 1965.

[16] TR Kirkpatrick and D Thirumalai. Colloquium: Random first order transition theory concepts in biology and physics. *Reviews of Modern Physics*, 87(1):183, 2015.

[17] Rodney D Priestley, Christopher J Ellison, Linda J Broadbelt, and John M Torkelson. Structural relaxation of polymer glasses at surfaces, interfaces, and in between. *Science*, 309(5733):456–459, 2005.

[18] Simone Napolitano, Emmanouil Glynos, and Nicholas B Tito. Glass transition of polymers in bulk, confined geometries, and near interfaces. *Reports on Progress in Physics*, 80(3):036602, 2017.

[19] Ronald P White and Jane EG Lipson. To understand film dynamics look to the bulk. *Physical Review Letters*, 125(5):058002, 2020.

[20] Z Fakhraai and JA Forrest. Measuring the surface dynamics of glassy polymers. *Science*, 319(5863):600–604, 2008.

[21] Rintaro Inoue, Toshiji Kanaya, Takeshi Yamada, Kaoru Shibata, and Koji Fukao. Experimental investigation of the glass transition of polystyrene thin films in a broad frequency range. *Physical Review E*, 97(1):012501, 2018.

[22] Virginie M Boucher, Daniele Cangialosi, Huajie Yin, Andreas Schönhals, Angel Alegría, and Juan Colmenero. T g depression and invariant segmental dynamics in polystyrene thin films. *Soft Matter*, 8(19):5119–5122, 2012.

[23] Koji Fukao and Yoshihisa Miyamoto. Glass transition temperature and dynamics of α-process in thin polymer films. *EPL (Europhysics Letters)*, 46(5):649, 1999.

[24] PA O'connell and GB McKenna. Rheological measurements of the thermoviscoelastic response of ultrathin polymer films. *Science*, 307(5716):1760–1763, 2005.

[25] Christopher J Ellison, Robert L Ruszkowski, Nathaniel J Fredin, and John M Torkelson. Dramatic reduction of the effect of nanoconfinement on the glass transition of polymer films via addition of small-molecule diluent. *Physical review letters*, 92(9):095702, 2004.

[26] Haonan Wang, Jyo Lyn Hor, Yue Zhang, Tianyi Liu, Daeyeon Lee, and Zahra Fakhraai. Dramatic increase in polymer glass transition temperature under extreme nanoconfinement in weakly interacting nanoparticle films. *ACS nano*, 12(6):5580–5587, 2018.

[27] Yue Zhang and Zahra Fakhraai. Decoupling of surface diffusion and relaxation dynamics of molecular glasses. *Proceedings of the National Academy of Sciences*, 114(19):4915–4919, 2017.

[28] Yue Zhang, Richard Potter, William Zhang, and Zahra Fakhraai. Using tobacco mosaic virus to probe enhanced surface diffusion of molecular glasses. *Soft Matter*, 12(44):9115–9120, 2016.

[29] Wei Zhang and Lian Yu. Surface diffusion of polymer glasses. *Macromolecules*, 49(2):731–735, 2016.

[30] Mithun Chowdhury, Paul Freyberg, Falko Ziebert, Arnold C-M Yang, Ullrich Steiner, and Günter Reiter. Segmental relaxations have macroscopic consequences in glassy polymer films. *Physical review letters*, 109(13):136102, 2012.

[31] Hamed Emamy, Sanat K Kumar, and Francis W Starr. Diminishing interfacial effects with decreasing nanoparticle size in polymer-nanoparticle composites. *Physical Review Letters*, 121(20):207801, 2018.

[32] Jean-Louis Barrat, Jörg Baschnagel, and Alexey Lyulin. Molecular dynamics simulations of glassy polymers. *Soft Matter*, 6(15):3430–3446, 2010.

[33] Günter Reiter and Simone Napolitano. Possible origin of thickness-dependent deviations from bulk properties of thin polymer films. *Journal of Polymer Science Part B: Polymer Physics*, 48(24):2544–2547, 2010.

[34] Peter Vandenabeele. *Practical Raman spectroscopy: an introduction*. John Wiley & Sons, 2013.

[35] Richard Zallen. *The physics of amorphous solids*. John Wiley & Sons, 2008.

[36] John M Chalmers and Peter R Griffiths. *Handbook of vibrational spectroscopy*. Wiley, 2002.

[37] John Chalmers and Peter Griffiths. *Handbook of Vibrational Spectroscopy, 5 volumes set*. Wiley, 2002.

[38] Jacob D Stevenson, Jörg Schmalian, and Peter G Wolynes. The shapes of cooperatively rearranging regions in glass-forming liquids. *Nature Physics*, 2(4):268–274, 2006.

[39] Mark D Ediger, C Austen Angell, and Sidney R Nagel. Supercooled liquids and glasses. *The journal of physical chemistry*, 100(31):13200–13212, 1996.

[40] Jing Zhao and Gregory B McKenna. Temperature divergence of the dynamics of a poly (vinyl acetate) glass: Dielectric vs. mechanical behaviors. *The Journal of chemical physics*, 136(15):154901, 2012.

[41] Yichen Guo, Shan He, Kai Yang, Yuan Xue, Xianghao Zuo, Yingjie Yu, Ying Liu, Chung-Chueh Chang, and Miriam H Rafailovich. Enhancing the mechanical properties of biodegradable polymer blends using tubular nanoparticle stitching of the interfaces. *ACS applied materials & interfaces*, 8(27):17565–17573, 2016.

[42] M Tyagi, A Arbe, F Alvarez, J Colmenero, and MA Gonzalez. Short-range order and collective dynamics of poly (vinyl acetate): A combined study by neutron scattering and molecular dynamics simulations. *The Journal of chemical physics*, 129(22):224903, 2008.

[43] Smarajit Karmakar, Chandan Dasgupta, and Srikanth Sastry. Growing length scales and their relation to timescales in glass-forming liquids. *Annu. Rev. Condens. Matter Phys.*, 5(1):255–284, 2014.

[44] K Hima Nagamanasa, Shreyas Gokhale, AK Sood, and Rajesh Ganapathy. Direct measurements of growing amorphous order and non-monotonic dynamic correlations in a colloidal glass-former. *Nature Physics*, 11(5):403–408, 2015.